BOLD and EEG Signal Variability at Rest Differently Relate to Aging in the Human Brain

D. Kumral[1,2], F. Şansal[3,1], E. Cesnaite[1], K. Mahjoory[1,4], E. Al[2,1], M. Gaebler[1,2], V. V. Nikulin[1,5,6], A. Villringer[1,2,7,8]

[1]Department of Neurology, Max Planck Institute for Human Cognitive and Brain Sciences, Leipzig, Germany
[2]MindBrainBody Institute at the Berlin School of Mind and Brain, Humboldt-Universität zu Berlin, Berlin, Germany
[3]International Graduate Program Medical Neurosciences, Charité-Universitätsmedizin, Berlin, Germany
[4]Institute for Biomagnetism and Biosignalanalysis, University of Muenster, Muenster, Germany
[5]Neurophysics Group, Department of Neurology, Campus Benjamin Franklin, Charité Universitätsmedizin Berlin, Berlin, Germany
[6]Centre for Cognition and Decision Making, National Research University Higher School of Economics, Moscow, Russian Federation
[7]Center for Stroke Research Berlin, Charité – Universitätsmedizin Berlin, Berlin, Germany
[8]Department of Cognitive Neurology, University Hospital Leipzig

Corresponding author: Deniz Kumral, Department of Neurology, Max Planck Institute for Human Cognitive and Brain Sciences, Stephanstrasse 1A, 04103, Leipzig, Germany.
Email: dkumral@cbs.mpg.de

Abbreviations: BOLD – Blood Oxygenation Level Dependent; CBF – cerebral blood flow; CBV– cerebral blood volume; CCA – canonical correlation analysis; $CMRO_2$ – cerebral metabolic rate of oxygen; CVR – cerebrovascular reactivity; DMN – Default Mode Network; EEG – electroencephalography; EC – eyes closed; EO – eyes open; framewise displacement – FD; FDR - false discovery rate; FEM – finite element method; fMRI – functional Magnetic Resonance Imaging; fNIRS – functional Near-Infrared Spectroscopy; FWHM – full-width half-maximum; ICBM – International Consortium for Brain Mapping; MEG – magnetoencephalography; MNI – Montreal Neurological Institute; rho – Spearman's rank correlation coefficient; PET –Positron-emission tomography; ROI – regions of interests; rs – resting state; SD – standard deviation; SVD – Singular Value Decomposition; TIV–Total Intracranial Volume

Abstract

Variability of neural activity is regarded as a crucial feature of healthy brain function, and several neuroimaging approaches have been employed to assess it noninvasively. Studies on the variability of both evoked brain response and spontaneous brain signals have shown remarkable changes with aging but it is unclear if the different measures of brain signal variability – identified with either hemodynamic or electrophysiological methods – reflect the same underlying physiology. In this study, we aimed to explore age differences of spontaneous brain signal variability with two different imaging modalities (EEG, fMRI) in healthy younger (25±3 years, N=135) and older (67±4 years, N=54) adults. Consistent with the previous studies, we found lower blood oxygenation level dependent (BOLD) variability in the older subjects as well as less signal variability in the amplitude of low-frequency oscillations (1–12 Hz), measured in source space. These age-related reductions were mostly observed in the areas that overlap with the default mode network. Moreover, age-related increases of variability in the amplitude of beta-band frequency EEG oscillations (15–25 Hz) were seen predominantly in temporal brain regions. There were significant sex differences in EEG signal variability in various brain regions while no significant sex differences were observed in BOLD signal variability. Bivariate and multivariate correlation analyses revealed no significant associations between EEG- and fMRI-based variability measures. In summary, we show that both BOLD and EEG signal variability reflect aging-related processes but are likely to be dominated by different physiological origins, which relate differentially to age and sex.

Keywords: brain signal variability, resting state, BOLD, fMRI, EEG, aging, sex, default mode network

1. Introduction

Functional neuroimaging methods such as fMRI, PET, fNIRS, EEG, or MEG have allowed the non-invasive assessment of functional changes in the aging human brain (Cabeza, 2001; Cabeza et al., 2018). Most previous functional neuroimaging studies on aging have employed a task-based design (Grady, 2012) and in their data analysis the central tendency has typically been assumed to be the most representative value in a distribution (e.g., mean) (Speelman and McGann, 2013) or the "signal" within distributional "noise". In recent years, also the variability of brain activation in task-dependent and task-independent measurements (as spontaneous variations of background activity) has been shown to provide relevant information about the brain's functional state (Garrett et al., 2013b; Grady and Garrett, 2018; Nomi et al., 2017). These studies primarily measured the blood oxygen level dependent (BOLD) signal using fMRI. For example, it has been demonstrated that the variance of the task-evoked BOLD response was differentially related to aging as well as cognitive performance (Armbruster-Genc et al., 2016; Garrett et al., 2013a). Similarly, spontaneous signal variability in resting state fMRI (rsfMRI) has been found to decrease with age (Grady and Garrett, 2018; Nomi et al., 2017), in individuals with stroke (Kielar et al., 2016), and 22q11.2 deletion syndrome (Zöller et al., 2017). An increase of fMRI variability has been shown to occur in inflammation induced state-anxiety (Labrenz et al., 2018) and to parallel symptom severity in Attention Deficit Hyperactivity Disorder (Nomi et al., 2018). From these studies, it was concluded that changes in BOLD signal variability might serve as an index for alterations in neural processing and cognitive flexibility (Grady and Garrett, 2014).

The conclusions of aforementioned studies imply that BOLD signal variability is mainly determined by *neuronal* variability. To a large extent, this is based on the premise that BOLD is related to neuronal activity: The evoked BOLD signal in task-based fMRI reflects the decrease of the deoxyhemoglobin concentration to changes in local brain activity, which is determined by vascular (blood velocity and volume: "neurovascular coupling") and metabolic (oxygen consumption: "neurometabolic coupling") factors (Logothetis and Wandell, 2004; Villringer and Dirnagl, 1995). The BOLD signal is therefore only an indirect measure of neural activity (Logothetis, 2008). For the variability of task-evoked BOLD signal and for spontaneous variations of the BOLD signal, in principle, the same considerations apply regarding their relationship to underlying neural processes (Murayama et al., 2010). However, since in rsfMRI there is no explicit external trigger for evoked brain activity to which time-locked averaging could be applied, the time course of rsfMRI signals is potentially more susceptible to contributions of "physiological noise", such as cardiac and respiratory signals

(Birn et al., 2008; Chang et al., 2009), but also spontaneous fluctuations of vascular tone, which is found even in isolated arterial vessels (Failla et al., 1999; Hudetz et al., 1998; Wang et al., 2006). In the same vein, the variability of task-evoked fMRI is not necessarily reflecting only the variability of evoked neuronal activity, as it may also – at least partly – reflect the variability of the spontaneous background signal on which a constant evoked response is superimposed.

In aging, non-neuronal signal fluctuations may also introduce spurious common variance across the rsfMRI time series (Caballero-Gaudes and Reynolds, 2017), thus confounding estimates of "neural" brain signal variability. Previous evidence suggests that the relationship between neuronal activity and the vascular response is attenuated with age – and so is, as a consequence, the BOLD signal (for review see D'Esposito et al., 2003). For instance, aging has been associated with altered cerebrovascular ultrastructure, reduced elasticity of vessels, and atherosclerosis (Farkas and Luiten, 2001) but also with a decrease in resting cerebral blood flow (CBF), cerebral metabolic rate of oxygen ($CMRO_2$), and cerebrovascular reactivity (CVR) (Liu et al., 2013). Taken together, age-related changes in BOLD signal or BOLD signal variability are related to a mixture of alterations in non-neural spontaneous fluctuations of vascular signals, neural activity, neurovascular coupling, and/or neurometabolic coupling (D'Esposito et al., 2003; Geerligs et al., 2017; Tsvetanov et al., 2015).

While BOLD fMRI signal and specifically variance measures based on fMRI are only partially and indirectly related to neural activity (Liu, 2013; Logothetis, 2008), electrophysiological methods such as EEG can provide a more direct assessment of neural activity with a higher temporal but poorer spatial resolution (Cohen, 2017). EEG measures neuronal currents resulting from the synchronization of dendritic postsynaptic potentials across the neural population; the cerebral EEG rhythms thereby reflect the underlying brain neural network activity (Steriade, 2006). Resting state (rs)EEG is characterized by spontaneous oscillations ("brain rhythms") at different frequencies. Previously, the mean amplitude of low-frequency bands (e.g., delta and/or theta, 1-7 Hz) has been shown to correlate negatively with age (Vlahou et al., 2015), while higher-frequency bands (e.g., beta, 15-25 Hz) show the reverse pattern (Rossiter et al., 2014). However, less is known about the within-subject variability of EEG measures and their association with aging. Several studies have addressed the variability in the spectral amplitudes of different frequency bands using variance (Hawkes and Prescott, 1973; Oken and Chiappa, 1988), coefficient of variation (Burgess and Gruzelier, 1993; Maltez et al., 2004), and complexity (Fernández et al., 2012;

Sleimen-Malkoun et al., 2015). For instance, reductions of the complexity in rsEEG signal have been found not only in healthy aging (Yang et al., 2013; Zappasodi et al., 2015) but also in age-related pathologies such as mild cognitive impairment (McBride et al., 2014) and Alzheimer's disease (Smits et al., 2016). Accordingly, it has been suggested that irregular (e.g., variable) systems indicate a normal and healthy state (more integrated information) while highly regular systems often mark dysfunction or disease (Lipsitz and Goldberger, 1992; Vaillancourt and Newell, 2002).

The different methodological approaches, fMRI based "vascular" approaches on the one hand and electrophysiological methods such as EEG and MEG, on the other hand, indicate alterations of brain signal variability with aging. However, it remains unclear whether these different measures of brain variability at rest reflect the same underlying physiological changes. Evidently, there are some correlations between the two signal sources (for a review see, Jorge et al., 2014; Ritter and Villringer, 2006). For instance, in task-based EEG-fMRI simultaneous recordings, a relationship between BOLD responses and amplitude of evoked potentials has been demonstrated (e.g., Ritter et al., 2009; Seaquist et al., 2007), while in resting state EEG-fMRI studies, a negative association between spontaneous modulations of alpha rhythm and BOLD signal has also been established (e.g., Chang et al., 2013; Goldman et al., 2002; Gonçalves et al., 2006; Moosmann et al., 2003). Further, differential correlation patterns have been noted for the various rhythms of different frequencies in EEG/MEG and the fMRI signal, such that low-frequency oscillations show a negative (Deligianni et al., 2014; Mantini et al., 2007; Meyer et al., 2013), while higher frequencies oscillations demonstrate a positive correlation with the BOLD signal (Niessing et al., 2005; Scheeringa et al., 2011).

Regarding the known age-related changes in BOLD and EEG signal variability, respectively, the question arises whether these alterations are dominated by joint signal sources of fMRI and EEG or by – potentially different – signal contributions that relate to each of these two methods. Given the – potentially large – non-neuronal signal contribution, this issue is particularly relevant for rsfMRI studies. Here, we addressed this question by analyzing rsfMRI and EEG measures of variability in healthy younger and older subjects. To our knowledge, the only study that compared variability in a "vascular" imaging method (rsfMRI) and an electrophysiological method (rsMEG at the sensor space) concluded that the effects of aging on BOLD signal variability were mainly driven by vascular factors (e.g., heart rate variability) and not well-explained by the changes in neural variability (Tsvetanov et al., 2015). The main aims of the present study were to explore i) age differences of brain signal variability measures, as well as to investigate ii) how neural variability derived from rsEEG related to the analogous parameters of BOLD signal variability derived from rsfMRI. We used rsfMRI and rsEEG from the "Leipzig Study for Mind-Body-Emotion Interactions" (Babayan et al., 2019). As an explanatory analysis, we further investigated sex-related differences of brain signal variability measures. To measure brain signal variability, we calculated the standard deviation (SD) of both the BOLD signal and of the amplitude envelope of the filtered rsEEG time series for a number of standard frequency bands at the source space. We hypothesized that brain signal variability would generally decrease with aging. In addition, based on the premise that BOLD fMRI signal variability reflects *neural* variability as measured by rsEEG, we expected that the corresponding changes in both signal modalities would demonstrate moderate to strong similarity in their spatial distribution. Given the confounding effects of vascular factors during aging on the fMRI signal (D'Esposito et al., 2003; Liu, 2013; Thompson, 2018), we further expected to find the relationship between BOLD and EEG signal variability to be stronger in younger than older adults.

2. Method

2.1.Participants

The data of the "Leipzig Study for Mind-Body-Emotion Interactions" (LEMON; Babayan et al., 2019) comprised 227 subjects in two age groups (younger: 20-35, older: 59-77). Only participants who did not report any neurological disorders, head injury, alcohol or other substance abuse, hypertension, pregnancy, claustrophobia, chemotherapy and malignant diseases, current and/or previous psychiatric disease or any medication affecting the cardiovascular and/or central nervous system in a telephone pre-screening were invited to the laboratory. The study protocol conformed to the Declaration of Helsinki and was approved by the ethics committee at the medical faculty of the University of Leipzig (reference number 154/13-ff).

RsEEG recordings were available for 216 subjects who completed the full study protocol. We excluded data from subjects that had missing event information (N=1), different sampling rate (N=3), mismatching header files or insufficient data quality (N=9). Based on the rsfMRI quality assessment, we further excluded data from subjects with faulty preprocessing (N=7), ghost artefacts (N=2), incomplete data (N=1), or excessive head motion (N=3) (criterion: mean framewise displacement (FD) ≤ 0.5 mm; Power et al., 2012) (Supplementary Figure 1). The final sample included 135 younger (M = 25.10 ± 3.70 years, 42 females) and 54 older subjects (M = 67.15 ± 4.52 years, 27 females).

2.1.fMRI Acquisition

Brain imaging was performed on a 3T Siemens Magnetom Verio MR scanner (Siemens Medical Systems, Erlangen, Germany) with a standard 32-channel head coil. The participants were instructed to keep their eyes open and not fall asleep while looking at a low-contrast (light grey on dark grey background) fixation cross.

The structural image was recorded using an MP2RAGE sequence (Marques et al., 2010) with the following parameters: TI 1 = 700 ms, TI 2 = 2500 ms, TR = 5000 ms, TE = 2.92 ms, FA 1 = 4°, FA 2 = 5°, band width = 240 Hz/pixel, FOV = 256 × 240 × 176 mm^3, voxel size = 1 x 1 x 1 mm^3. The functional images were acquired using a T2*-weighted multiband EPI sequence with the following parameters: TR = 1400 ms, TE = 30 ms, FA= 69°, FOV = 202 mm, imaging matrix=88 × 88, 64 slices with voxel size = 2.3 x 2.3 x 2.3 mm^3, slice thickness = 2.3 mm, echo spacing = 0.67 ms, bandwidth=1776 Hz/Px, partial fourier 7/8, no pre-scan normalization, multiband acceleration factor = 4, 657 volumes, duration = 15 min 30 s. A gradient echo field map with the sample geometry was used for distortion correction (TR = 680 ms, TE 1 = 5.19 ms, TE 2 = 7.65 ms).

2.2. fMRI Preprocessing

Preprocessing was implemented in Nipype (Gorgolewski et al., 2011), incorporating tools from FreeSurfer (Fischl, 2012), FSL (Jenkinson et al., 2012), AFNI (Cox, 1996), ANTs (Avants et al., 2011), CBS Tools (Bazin et al., 2014), and Nitime (Rokem et al., 2009). The pipeline comprised the following steps: (I) discarding the first five EPI volumes to allow for signal equilibration and steady state, (II) 3D motion correction (FSL mcflirt), (III) distortion correction (FSL fugue), (IV) rigid body coregistration of functional scans to the individual T1-weighted image (Freesurfer bbregister), (V) denoising including removal of 24 motion parameters (CPAC, Friston et al., 1996), motion, signal intensity spikes (Nipype rapidart), physiological noise in white matter and cerebrospinal fluid (CSF) (CompCor; Behzadi et al., 2007), together with linear and quadratic signal trends, (VI) band-pass filtering between 0.01-0.1 Hz (FSL fslmaths), (VII) spatial normalization to MNI152 (Montreal Neurological Institute) standard space (2 mm isotropic) via transformation parameters derived during structural preprocessing (ANTS). (VIII) The data were then spatially smoothed with a 6-mm full-width half-maximum (FWHM) Gaussian kernel (FSL fslmaths). Additionally, we calculated total intracranial volume (TIV) of each subject using the Computational Anatomy Toolbox (CAT12: http:// dbm.neuro.uni-jena.de/cat/) running on Matlab 9.3 (Mathworks, Natick, MA, USA) and used it as a covariate for further statistical analyses (Malone et al., 2015).

BOLD Signal Variability (SD_{BOLD}). Standard deviation (SD) quantifies the amount of variation or dispersion in a set of values (Garrett et al., 2015; Grady and Garrett, 2018). Higher SD in rsfMRI signal indicates greater intensity of signal fluctuation or an increased level of activation in a given area (Garrett et al., 2011). We first calculated SD_{BOLD} across the whole time series for each voxel and then within 96 boundaries of preselected atlas-based regions of interests (ROIs) based on the Harvard-Oxford cortical atlas (Desikan et al., 2006). The main steps of deriving brain signal variability (SD_{BOLD}) from the preprocessed fMRI signal are shown in Figure 1.

The reproducible workflows containing fMRI preprocessing details can be found here: https://github.com/NeuroanatomyAndConnectivity/pipelines/releases/tag/v2.0.

2.3. EEG Recordings

Sixteen minutes of rsEEG were acquired on a separate day with BrainAmp MR-plus amplifiers using 61 ActiCAP electrodes (both Brain Products, Germany) attached according to the international standard 10-20 localization system (Jurcak et al., 2007) with FCz (fronto-central or cephalic electrode) as the reference. The ground electrode was located at the sternum. Electrode impedance was kept below 5 kΩ. Continuous EEG activity was digitized at a sampling rate of 2500 Hz and band–pass filtered online between 0.015 Hz and 1 kHz.

The experimental session was divided into 16 blocks, each lasting 60 s, with two conditions interleaved, eyes closed (EC) and eyes open (EO), starting with the EC condition. Changes between blocks were announced with the software Presentation (v16.5, Neurobehavioral Systems Inc., USA). Participants were asked to sit comfortably in a chair in a dimly illuminated, sound-shielded Faraday recording room. During the EO periods, participants were instructed to stay awake while fixating on a black cross presented on a white background. To maximize comparability, only EEG data from the EO condition were analyzed, since rsfMRI data were collected only in the EO condition.

2.4.EEG Data Analysis

EEG processing and analyses were performed with custom Matlab (The MathWorks, Inc, Natick, Massachusetts, USA) scripts using functions from the EEGLAB environment (version 14.1.1b; Delorme and Makeig, 2004). The continuous EEG data were down-sampled to 250 Hz, band-pass filtered within 1–45 Hz (4^{th} order back and forth Butterworth filter) and split into EO and EC conditions. Segments contaminated by large artefacts due to facial muscle tensions and gross movements were removed following visual inspection, resulting in a rejection of on average 6.6% of the recorded data. Rare occasions of artifactual channels were excluded from the analysis. The dimensionality of the data was reduced using principal component analysis (PCA) by selecting at least 30 principal components explaining 95% of the total variance. Next, using independent component analysis (Infomax; Bell and Sejnowski, 1995), the confounding sources e.g. eye-movements, eye-blinks, muscle activity, and residual ballistocardiographic artefacts were rejected from the data.

2.5.EEG Source Reconstruction

Before conducting source reconstruction, preprocessed EEG signals were re-referenced to a common average. We incorporated a standard highly detailed finite element method (FEM) volume conduction model as described by Huang et al. (2016).
The geometry of the FEM model was based on an extended MNI/ICBM152 (International Consortium for Brain Mapping) standard anatomy, where the source space constrained to cortical surface and parceled to 96 ROIs based on the Harvard-Oxford atlas (Desikan et al., 2006). We used eLORETA (exact low resolution brain electromagnetic tomography) as implemented in as implemented in as implemented in the M/EEG Toolbox of Hamburg (METH; Haufe and Ewald, 2016; Pascual-Marqui, 2007) to compute the cortical electrical distribution from the scalp EEG recordings. The leadfield matrix was calculated between

1804 points located on the cortical surface to the 61 scalp electrodes. We filtered into several frequency bands, associated with brain oscillations: delta (1−3 Hz), theta (4−8 Hz), alpha (8–12 Hz), and beta (15–25 Hz). Following the singular value decomposition (SVD) of each voxel's three-dimensional time course, the dominant orientation of the source signal was identified by preserving the first SVD component. The amplitude envelope of filtered oscillations was extracted using the Hilbert transform (Rosenblum et al., 2001). Next, we applied temporal coarse graining by averaging data points in non-overlapping windows of length 0.5 s (Figure 1).

EEG Variability (SD_{EEG}). We calculated the SD of amplitude envelope of band-pass filtered oscillations on the coarse-grained signal. RsEEG signal variability (SD_{EEG}) was obtained for different frequency bands (SD_{DELTA}, SD_{THETA}, SD_{ALPHA}, SD_{BETA}) in each of 96 ROIs. Further, in our study we investigated variability in the amplitude of oscillatory signals from one time segment to the other. If amplitude (or power) of each signal stays the same, the variability (SD) in the amplitude of such segments will be zero. Therefore, the average amplitude of a signal is not indicative of its variability. Although amplitude and its standard deviation mathematically are different, they can show some correlation due to size effects (Immer, 1937).

Main steps toward deriving brain signal variability from the preprocessed EEG signal are shown in Figure 1. The raw and preprocessed fMRI and EEG data samples can be found at https://ftp.gwdg.de/pub/misc/MPI-Leipzig_Mind-Brain-Body-LEMON/

Figure 1. Main steps of deriving brain signal variability from the preprocessed resting state fMRI and EEG signal. We calculated the standard deviation of the blood oxygen level dependent (BOLD) signal and of the coarse-grained amplitude envelope of the rsEEG time series for a number of standard frequency bands at the source space. Each sample of coarse-grained amplitude envelope of the rsEEG (represented in numbers) is generated by averaging the samples in non-overlapping windows of length 0.5 s.

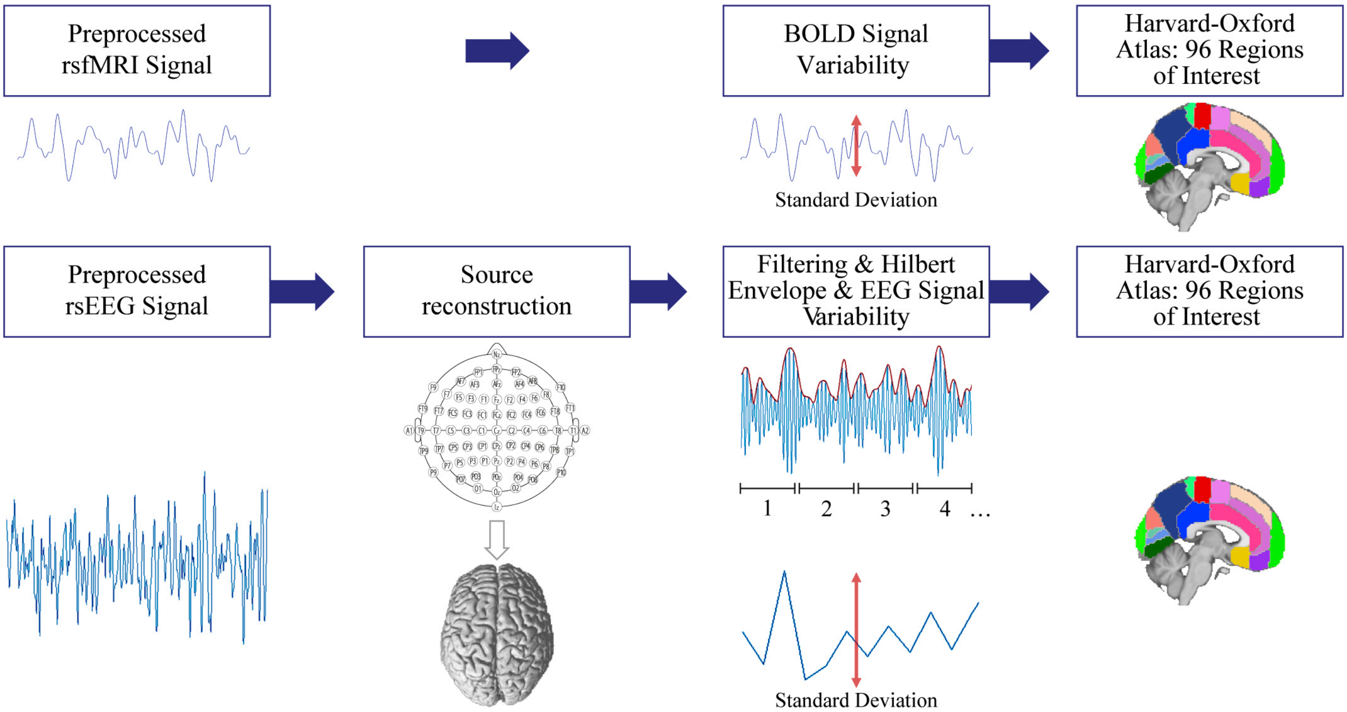

2.6. Statistical Analyses

Mean SD_{BOLD} and SD_{EEG}. For the topographic information (based on ROIs), the mean BOLD and EEG variability were calculated by I) log-transforming the SD values, II) averaging separately for younger and older subjects, and III) then back-transforming the values (McDonald, 2014).

Age and Sex Effects. A series of non-parametric analyses of covariance (ANCOVAs, type III) were applied to brain signal variability values in each 96 ROIs for SD_{BOLD} and SD_{EEG} using age group and sex as variables of interest, adjusting for TIV and mean FD. The significance level was controlled for using false discovery rate (FDR) correction according to Benjamini and Hochberg (1995). Significant group differences were further examined by Tukey HSD post-hoc comparisons. The signal variability values were log-transformed to normalize SD_{BOLD} and SD_{EEG} before further analyses (assessed by Lilliefors tests at a significance threshold of 0.05). All analyses were performed using the *aovp* function in the *lmperm* package (Wheeler, 2016) as implemented in R (R core team, 2018).

SD_{BOLD} – SD_{EEG} Correlation. To investigate the association between each ROI of SD_{BOLD} and SD_{EEG}, we used pairwise Spearman's rank correlation separately for younger and older subjects, corrected for FDR (96 ROIs). We further applied sparse canonical correlation analysis (CCA) to show that the relationship between SD_{BOLD} and SD_{EEG} is not missed when only mass bivariate correlations are used. CCA is a multivariate method to find the independent linear combinations of variables such that the correlation between variables is maximized (Witten et al., 2009). The sparse CCA criterion is obtained by adding a Lasso Penalty function (l_1), which performs continuous shrinkage and automatic variable selection and can solve statistical problems such as multicollinearity and overfitting (Tibshirani, 2011). We used l_1 penalty as the regularization function to obtain sparse coefficients, that is, the canonical vectors (i.e., translating from full variables to a data matrix's low-rank components of variation) will contain exactly zero elements. Sparse CCA was performed using the R package PMA (Penalized Multivariate Analysis; Witten et al., 2009; http://cran.r-project.org/web/packages/PMA/). In our analyses, the significance of the correlation was estimated using the permutation approach (N=1000) as implemented in the CCA.permute function in R (p_{perm}<0.05).

Cognition. The Trail Making Test (TMT) is a cognitive test measuring executive function, including processing speed and mental flexibility (Reitan, 1955; Reitan and Wolfson, 1995). In the first part of the test (TMT-A) the targets are all numbers, while in the second part (TMT-B), participants need to alternate between numbers and letters. In both TMT-A and B, the time to complete the task quantifies the performance, and lower scores indicate better performance. Based on the previous literature, we focused on SD_{BOLD}, SD_{DELTA}, and SD_{THETA} (Vlahou et al., 2015) and selected different ROIs from two research papers about the neural correlates of the TMT: Zakzanis et al., (2005) and Jacobson et al., (2011) (Table 1). To reduce the number of multiple comparisons (Nguyen and Holmes, 2019), these ROIs were decomposed into singular values using the *prcomp* function belonging to *factoextra* package (R core team, 2018), which performs SVD on the centered values. As a criterion, the minimum total variance explained over 70% was selected (Jollife and Cadima, 2016). This resulted in three principle components (PC) in SD_{BOLD} (52.82%, 10.34%, and 7%), two PCs in SD_{DELTA} (67.37%, 10.95%), and one PC in SD_{THETA} (75.63%). We also ran multiple linear regression using task completion time in TMT-A and TMT-B as the dependent variables with the PC scores (for SD_{BOLD}, SD_{DELTA}, and SD_{THETA}) and their interaction with continuous age as independent variables. Since the residuals from the regression models fitted to the data were not normally distributed, the TMT values were log-transformed prior to the final analyses. These tests were conducted using the *lmp* function in *lmperm* package implemented in R (R core team, 2018).

Table 1. Selected region of interests (ROIs) derived from the previous fMRI literature, and their corresponding ROIs in Harvard-Oxford atlas to investigate the age-dependent relationship between TMT and SD_{BOLD} or SD_{EEG}.

Literature	Region	Hemisphere	Harvard-Oxford Atlas
Zakzanis et al., 2005	Middle Frontal Gyrus	Left	Middle Frontal Gyrus
	Precentral Gyrus	Left	Precentral Gyrus
	Cingulate Gyrus	Left/Right	Cingulate Gyrus, anterior/posterior
	Superior Frontal Gyrus	Left	Superior Frontal Gyrus
	Medial Frontal Gyrus	Left	Frontal Medial Cortex
	Insula	Left/Right	Insular Cortex
	Middle Temporal Gyrus	Left	Middle Temporal Gyrus, anterior/posterior/temporooccipital
	Superior Temporal Gyrus	Left	Superior Temporal Gyrus, anterior/posterior
Jacobson et al., 2011	Fusiform Gyrus	Right	Occipital Fusiform Gyrus
	Inferior Middle Frontal Gyrus	Right	Middle Frontal Gyrus
	Precentral Gyrus	Right	Precentral Gyrus

3. Results

Mean SD_{BOLD} and SD_{EEG}. The topographic distribution of SD_{BOLD} in younger adults revealed the largest brain signal variability values in fronto-temporal regions while in older adults it was in the frontal and occipital areas. Further, we found strongest variability across younger subjects in occipito-temporal regions for SD_{DELTA}, SD_{THETA}, SD_{ALPHA}, and in medial frontal brain regions for SD_{BETA}, while older adults showed strongest brain signal variability in the fronto-central brain regions for SD_{DELTA}, in parietal-central brain regions for SD_{THETA}, SD_{ALPHA}, and in medial frontal brain regions for SD_{BETA}. The details of the mean values of SD_{BOLD} and SD_{EEG} across age groups and their topographic distributions are given in Supplementary Table 1, Supplementary Figure 2 and 3, and are also available at Neurovault (https://neurovault.org/collections/WWOKVUDV/).

Age and Sex Effects. The nonparametric ANCOVAs with SD_{BOLD} as dependent variable demonstrated that there was a significant main effect of age group in 72 ROIs in frontal, temporal, and occipital brain regions (F-values: 13.32–61.14; Figure 2). However, there was no significant main effect of sex on SD_{BOLD} and no significant interaction between age group and sex (all $p_{FDR}>0.05$). Tukey HSD post-hoc analyses showed that older subjects had decreased SD_{BOLD} compared to younger adults which were presented in both sexes ($n_{ROI}=35$). The nonparametric ANCOVAs with SD_{EEG} as dependent variable showed significant main effects of age group in all frequency bands: SD_{DELTA} in 14 ROIs in occipital (F-values: 12.57–20.94), SD_{THETA} in 16 ROIs in frontal and parietal (F-values: 13.16–40.30), SD_{ALPHA} in 20 ROIs in occipital (F-values: 12.69–20.12), and SD_{BETA} in 19 ROIs in central and temporal brain regions (F-values: 12.50–21.61), as shown in Figure 2. There were also significant main effects of sex in all frequency bands: SD_{DELTA} in 21 ROIs in temporal and occipital (F-values: 13.24–26.63), SD_{THETA} in 74 ROIs in frontal, occipital, and temporal (F-values: 12.68–30.06), SD_{ALPHA} in 4 ROIs in frontal (F-values: 12.88–16.51), and SD_{BETA} in 69 ROIs in temporal, occipital, and central brain regions (F-values: 12.54–35.72), as shown in Figure 3. No significant interaction effects between age group and sex on SD_{EEG} were observed in any frequency band ($p_{FDR}>0.05$). Tukey HSD post-hoc analyses on SD_{EEG} showed that older subjects had less brain signal variability, which was present in both sexes for SD_{DELTA} ($n_{ROI}=12$), SD_{THETA} ($n_{ROI}=10$), and SD_{ALPHA} ($n_{ROI}=11$). Additionally, older adults showed higher SD_{BETA}, driven by female subjects ($n_{ROI}=15$). With regard to sex differences, post-hoc analyses showed that females had higher SD_{DELTA}, SD_{THETA}, SD_{ALPHA}, and SD_{BETA} than males. Sex differences in SD_{DELTA} ($n_{ROI}=13$) and SD_{THETA} ($n_{ROI}=54$) were mostly pronounced in younger adults, while the effect of sex in SD_{BETA} (n_{ROI}=21) were mainly presented in older adults ($p<0.05$). The graphical distribution of the F-values for the significant effects of age group or sex for each ROIs are shown in Supplementary Figure 4. Additional information of SD_{BOLD} and SD_{EEG} for each frequency band and for each of the 96 ROIs, split up by age group and sex, are presented in the Supplementary Tables 2-6.

Figure 2. Spatial maps of significant age group differences in SD_{BOLD} and SD_{EEG}. We calculated the standard deviation (SD) of the blood oxygen level dependent (BOLD) signal and of the coarse-grained amplitude envelope of the rsEEG time series for the delta (1–3 Hz), theta (4–8 Hz), alpha (8–12 Hz), and beta (15–25 Hz) frequency bands at the source space. Statistical significance was determined using nonparametric ANCOVAs corrected for multiple comparisons by false discovery rates (FDR; Benjamini and Hochberg, 1995). Blue color indicates areas where brain signal variability was lower in older than in younger adults, while red color indicates the opposite.

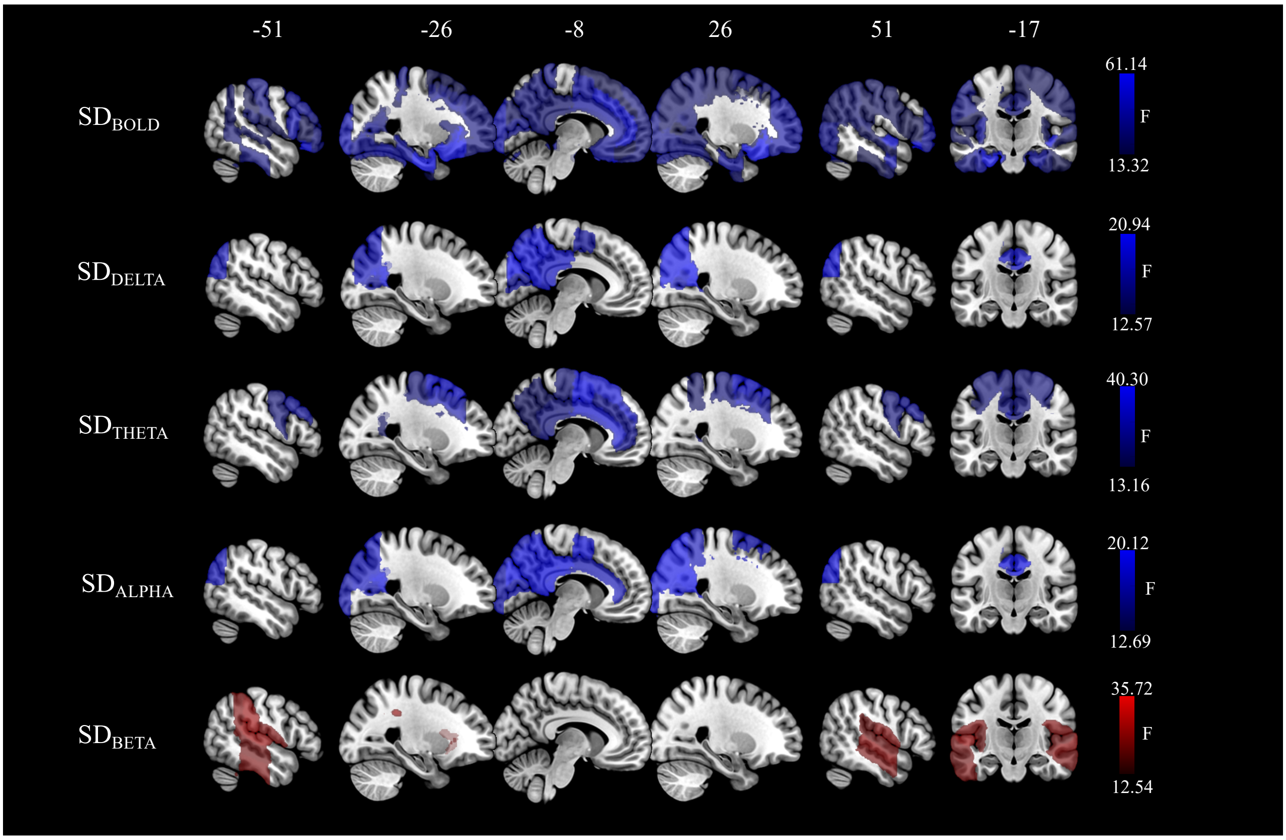

Figure 3. Spatial maps of significant sex differences in SD_{BOLD} and SD_{EEG}. We calculated the standard deviation (SD) of the blood oxygen level dependent (BOLD) signal and of the coarse-grained amplitude envelope of the rsEEG time series for the delta (1–3 Hz), theta (4–8 Hz), alpha (8–12 Hz), and beta (15–25 Hz) frequency bands at the source space. Statistical significance was determined using nonparametric ANCOVAs corrected for multiple comparisons by false discovery rates (FDR; Benjamini and Hochberg, 1995). Yellow color indicates areas where brain signal variability was higher in female subjects as compared to male subjects in EEG.

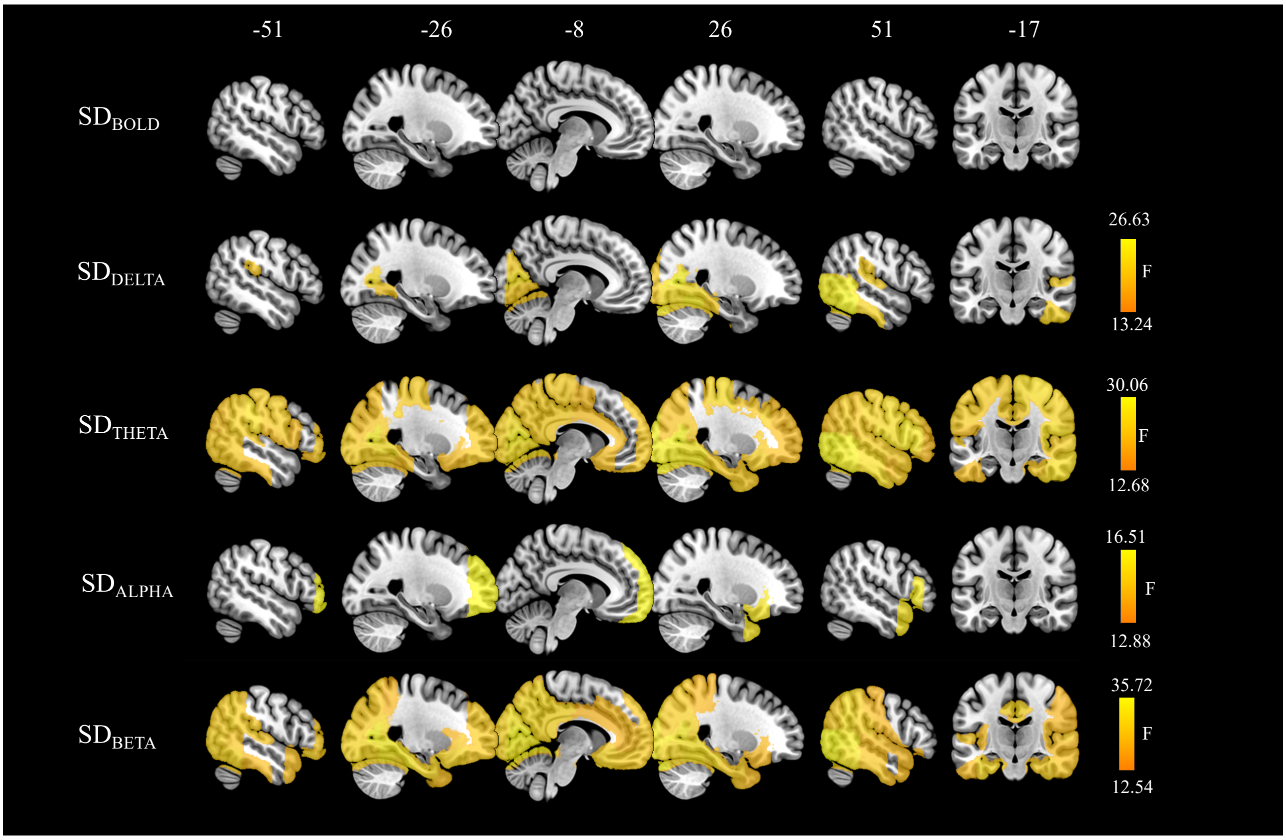

$SD_{BOLD} – SD_{EEG}$ Correlation. The correlation coefficient of pairwise associations for 96 ROIs of SD_{BOLD} with SD_{DELTA}, SD_{THETA}, SD_{ALPHA}, and SD_{BETA} ranged in younger adults from rho=-0.200 to rho=0.223 (Supplementary Table 7) and in older adults from rho=0.386 to rho=0.349 (Supplementary Table 8). None of the pairwise associations between SD_{BOLD} and SD_{EEG} remained significant after the correction for multiple comparison corrections. Confirmatory multivariate sparse CCA further showed that correlations between SD_{BOLD} and SD_{EEG} across all subjects were rather low, highly sparse, and non-significant (SD_{DELTA}; r=0.145, p_{perm} =0.750, l_1=0.367; SD_{THETA}; r=0.143, p_{perm}=0.713 l_1=0.7; SD_{ALPHA}; r=0.153, p_{perm}=0.528, l_1=0.1; SD_{BETA}; r=0. 232, p_{perm}=0.096, l_1=0.633).

Figure 4. Distribution of correlation coefficients (rho) for the association between SD_{BOLD} and SD_{EEG} for A) younger (N=135) and B) older (N=54) adults for different frequency bands across each pair of 96 regions of interests. The correlations between SD_{BOLD} and SD_{EEG} were tested using pairwise Spearman's rank correlation corrected for multiple comparison by false discovery rates (FDR; Benjamini and Hochberg, 1995).

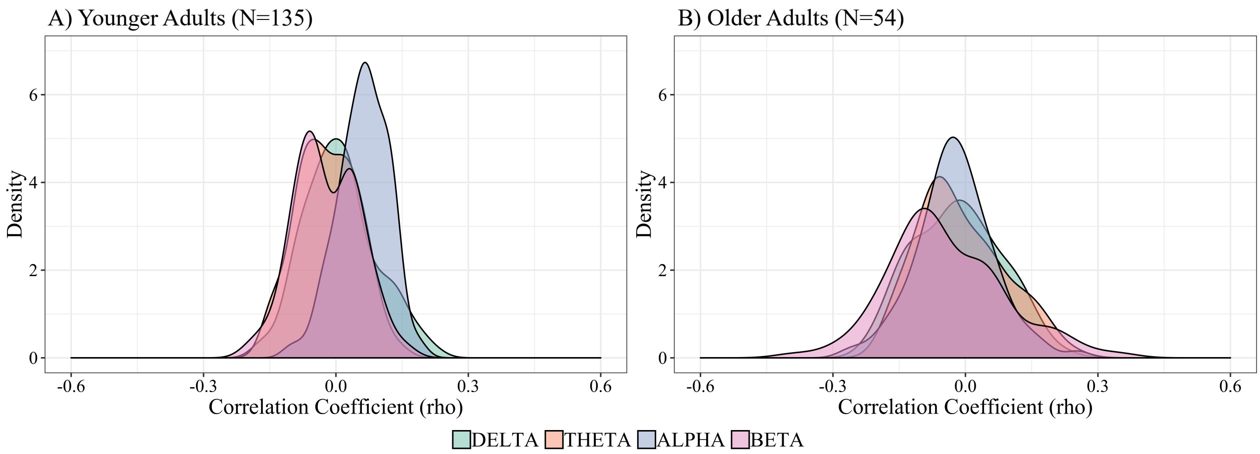

Cognition. There was a significant interaction between age and SD_{BOLD} in PC2 on the TMT-B performance (adjusted $R^2 = 0.395$, $F(7,181) = 18.60$, $p < .001$, interaction: $\beta = -0.002$, $p = 0.027$). For older, but not younger participants, stronger SD_{BOLD} was associated with faster completion time in PC2, driven mainly by the left temporal gyrus as well as the left anterior and posterior cingulate cortex (Figure 5). The regression analyses in SD_{DELTA} and SD_{THETA} did not show a significant association between cognition and brain signal variability measures. The contributions of selected ROIs to the PCs resulted from SVD analyses can be found in Supplementary Table 9. The complete multiple linear regression results can be found in Supplementary Table 10.

Figure 5. Age-dependent relationship between cognitive performance and BOLD signal variability.
The scatterplot shows the significant association between task completion time in TMT-B (x-axis) and SD_{BOLD} (adjusted $R^2 = 0.395$, $F(7,181) = 18.60$, $p < .001$, interaction: $\beta = -0.002$, $p = 0.027$) in PC2, driven mainly by the left anterior and posterior temporal gyrus, bilateral anterior and posterior cingulate cortex.

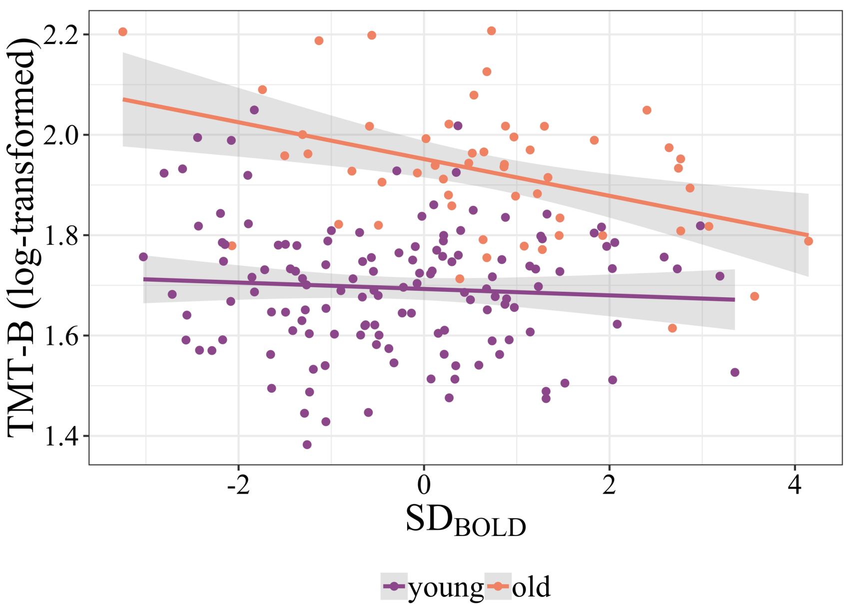

4. Discussion

Comparing healthy younger and older adults, we found widespread variability reductions in BOLD signal as well as in the amplitude envelope of delta, theta, and alpha frequency of rsEEG, whereas increased variability with aging was observed in the beta-band frequency. As a complementary analysis, we also explored sex differences and found that female subjects exhibited higher EEG signal variability than male subjects; no significant sex differences were found in BOLD signal variability. There were no significant correlations between hemodynamic (SD_{BOLD}) and electrophysiological (SD_{EEG}) measures of brain signal variability, neither in the younger nor in the older adults. Our results suggest that variability measures of rsfMRI and rsEEG – while both related to aging – are dominated by different physiological origins and relate differently to age and sex.

4.1. BOLD Signal Variability

The first aim of our study was to investigate the effect of age on BOLD signal variability, as measured by SD of spontaneous fluctuations during rsfMRI. Consistent with recent rsfMRI studies demonstrating that BOLD signal variability decreases with age in large-scale networks (Grady and Garrett, 2018; Nomi et al., 2017), we found that older subjects had reduced SD_{BOLD} in temporal and occipital brain regions but also in cortical midline structures like the precuneus, anterior and posterior cingulate cortices, as well as orbitofrontal cortex compared to younger adults. These age-related reductions in BOLD signal variability were thus especially apparent in regions of the Default Mode (DMN) and the Fronto-Parietal Network (FPN). The DMN is an intrinsically correlated network of brain regions, that is particularly active during rest or fixation blocks (Biswal et al., 2010). It reflects the systematic integration of information across the cortex (Margulies et al., 2016) and has been frequently associated with psychological functions like self-referential thought or mind-wandering, and also memory retrieval (Andrews-Hanna et al., 2014; Raichle, 2015). The FPN is involved in cognitive control processes (Spreng et al., 2013), and closely interacts with the DMN, for example during mind-wandering state (Golchert et al., 2017). Previous studies in healthy aging noted that older subjects showed lower functional connectivity in DMN and FPN regions (Damoiseaux, 2017; Damoiseaux et al., 2008; Meunier et al., 2009; Petersen et al., 2014). Similarly, an altered functional connectivity in the DMN has been found in different pathologies, for example, in Alzheimer's disease (Greicius et al., 2004) or mild cognitive impairment (Das et al., 2015). Further, we found a significant interaction between age and SD_{BOLD} in temporal and cingulate cortices for performance on the cognitive task (TMT-B), suggesting that the relationship between brain signal variability and cognitive performance depends on the participants' age. We speculate that – in the elderly – reduced BOLD signal variability in the DMN and the FPN, particularly in the overlapping frontal brain regions, could be related to locally impaired function that is reflected in impaired cognitive performance (Campbell et al., 2012). Such findings support the notion that local BOLD signal variability may be a valuable biomarker of neurocognitive health (and disease) in aging.

Sex-specific differences in brain structure and function have been previously shown (for a review see, Gong et al., 2011; Ruigrok et al., 2014; Sacher et al., 2013). For example, larger total brain volume has been reported in male as compared to female subjects (Gong et al., 2011), whereas higher cerebral blood flow (Gur et al., 1982; Rodriguez et al., 1988) and stronger functional connectivity in the DMN (Tomasi and Volkow, 2012) were found in females. In our exploratory analysis, we did not find significant sex differences in BOLD signal variability when controlling for total intracranial volume as an approximation of overall brain size.

4.2. Electrophysiological Signal Variability

Measures of neural variability were derived from rsEEG for several main frequency bands (delta, theta, alpha, beta) as the standard deviation of their amplitude of envelope time series data, analogously to the BOLD signal variability. Multimodal imaging studies have shown that the amplitude envelope of neural oscillatory activity across frequency bands relates to different rsfMRI networks (Brookes et al., 2011; Deligianni et al., 2014), confirming the neurophysiological origin of the resting state networks measured with BOLD fMRI. Additionally, these studies also concluded that different frequency bands can be related to the same functional network, but also differentially to distinct networks (Brookes et al., 2011; Laufs et al., 2006; Mantini et al., 2007; Meyer et al., 2013). For instance, Mantini et. al. (2007) reported that the visual network is associated with all frequency bands except gamma rhythm, while the sensorimotor network is primarily associated with beta-band oscillations.

In our analysis, we found age-dependent EEG signal variability changes within networks which were associated with more than one frequency band, thus confirming that neurons generating oscillations at different frequencies may contribute to the same network. More precisely, we found age-related reductions in SD_{DELTA} and SD_{ALPHA} mainly in a visual network (including calcarine regions, cuneal cortex, and occipital pole), SD_{THETA} in posterior DMN (e.g., posterior cingulate cortex), while an enhancement of SD_{BETA} was mainly seen in the temporal (e.g., superior/middle temporal gyrus), and central/sensorimotor (e.g., supramarginal gyrus) regions. These results align with previous reports of age-dependent changes of electrophysiological activity using spectral power (Dustman et al., 1993; Vlahou et al., 2015), and signal variability (Dustman et al., 1999; Tsvetanov et al., 2015).

Age-related decreases of alpha amplitude and alpha band variability (measured by SD of the oscillatory signal) were previously found in posterior and occipital brain regions (Babiloni et al., 2006; Tsvetanov et al., 2015). Alpha rhythm is a classical EEG hallmark of resting wakefulness (Laufs et al., 2003) that is modulated by thalamo-cortical and cortico-cortical interactions (Bazanova and Vernon, 2014; Goldman et al., 2002; Lopes Da Silva et al., 1997; Moosmann et al., 2003). It has been suggested that the posterior alpha-frequency plays an important role in the top-down control of cortical activation and excitability (Klimesch, 1999). Accordingly, decreased alpha variability in occipital regions might be associated with altered functioning of the cholinergic basal forebrain, affecting thalamo-cortical and cortico-cortical processing. Our finding of higher temporal and sensorimotor SD_{BETA} in the elderly is in line with previous findings (Rossiter et al., 2014; Tsvetanov et al., 2015). Aging has previously been associated with an increase in movement-related beta-band attenuation, suggesting an enhanced motor cortex GABAergic inhibitory activity in older individuals (Rossiter et al., 2014). Similarly, beta-band activity is thought to play a key role in signaling maintenance of the status quo of the motor system, despite the absence of movement (Engel and Fries, 2010). Therefore, greater SD_{BETA} in sensorimotor brain regions could be interpreted as a compensatory mechanism to account for a decline of motor performance during aging (Quandt et al., 2016).

It should be noted that the present findings of age-related alterations of brain signal variability at different frequencies might be influenced by several anatomical factors which might influence EEG-generators such as reduced cortical gray matter (Babiloni et al., 2013; Moretti et al., 2012), white-matter (Nunez et al., 2015; Valdés-Hernández et al., 2010), and increased amount of cerebrospinal fluid (CSF; Hartikainen et al., 1992; Stomrud et al., 2010), but also alterations of cerebral glucose metabolism (Dierks et al., 2000). Localized or global disturbances of brain anatomy and function might lead to deviations in the EEG sources, resulting in EEG amplitude changes. A methodological improvement for future studies will therefore be the application of individual head models (Ziegler et al., 2014).

In addition to the effect of age on rsEEG signal variability, an exploratory analysis showed sex differences in distinct brain regions and EEG frequencies. More precisely, we found higher SD_{DELTA} and SD_{THETA} in occipito-temporal, SD_{ALPHA} in frontal, and SD_{BETA} in frontal as well as occipito-temporal brain regions in female compared to male subjects. While some studies demonstrated higher alpha (Aurlien et al., 2003), delta (Armitage, 1995), theta (Carrier et al., 2001; Duffy et al., 1993), and beta power (Jaušovec and Jaušovec, 2010; Matsuura et al., 1985; Veldhuizen et al., 1993) in female relative to male subjects, other studies reported the opposite pattern (Brenner et al., 1995; Latta et al., 2005; Zappasodi et al., 2006). These differences in EEG signal variability could be a result of different mechanisms (biological/hormonal, cultural or developmental) involved in shaping sex differences. Unfortunately, based on our dataset we cannot differentiate which of these potential mechanisms might be most relevant for the observed changes.

4.3. Association between BOLD and EEG Variability

We further assessed how neural variability in source-reconstructed rsEEG related to the analogous parameters of BOLD signal variability in rsfMRI using univariate and multivariate correlation analyses. Previously, simultaneous EEG-fMRI studies have shown meaningful relationships between fluctuations in EEG power, frequency, phase, and local BOLD changes (for a review see, Jorge et al., 2014; Ritter and Villringer, 2006). Due to age-related physiological (particularly cardiovascular) alterations in the brain, we expected the relationship between BOLD and EEG signal variability to be stronger in younger than older adults. However, in the present study, both univariate and multivariate analyses showed no significant correlations between SD_{BOLD} and SD_{EEG} neither in the younger nor in the older adults. This finding was supported by the distinct anatomical distributions of age-related changes in BOLD and EEG signal variability, that barely showed a spatial overlap, suggesting different underlying physiological processes. What could they be? Clearly, neuronal activity is the main signal source for EEG- and MEG recordings as well as for EEG/MEG-based variability measures. BOLD signal variability, however, can reflect both vascular and neural processes (Garrett et al., 2017). While neuronal activity clearly contributes to the BOLD signal at rest (Ma et al., 2016; Mateo et al., 2017), our results indicate, however, that neuronal activity which is captured by EEG (or more specifically by our EEG-based measures), is not the major determinant of BOLD variability in the resting state. Other factors that could contribute to BOLD variability are (i) neuronal activity which is not captured by EEG and (ii) non-neural factors such as vasomotion, or cardiac and respiratory signals (Murphy et al., 2013). In the elderly, additional factors related to the known morphological and functional changes of blood vessels as well as age-related metabolic changes are known to affect CBF (Ances et al., 2009; Martin et al., 1991), $CMRO_2$ (Aanerud et al., 2012), and CVR (Liu et al., 2013) and therefore are likely to also influence BOLD variability. Thus, given different underlying physiology, joint EEG and fMRI variability studies might provide complementary information for a comprehensive assessment of neuronal as well as vascular factors related to aging.

5. Limitations

There are several limitations of our study: EEG and MRI scans were not recorded simultaneously. Therefore, we could not directly relate the two signals in a cross-correlation analysis. Furthermore, EEG and MRI were performed with different body postures (fMRI; supine, EEG; seated) known to affect brain function, for example, changes in the amplitude of the EEG signal have been related to different body postures presumably due to the shifts in cerebrospinal fluid layer thickness (Rice et al., 2013). Similarly, other experimental (e.g., visual display; Nir et al., 2006), environmental (e.g., acoustic noise in MRI; Andoh et al., 2017; Cho et al., 1998) and subject-related factors (e.g., changes of vigilance; Tagliazucchi and Laufs, 2014; Wong et al., 2013) could have introduced unintended variations in our results (Yan et al., 2013) and the influence of these factors is probably not the same for the different methods, e.g., noise in MRI or poor "control" of vigilance in MRI. For instance, given the well-known relationship between vigilance or arousal and fMRI signal fluctuations (Bijsterbosch et al., 2017; Chang et al., 2016; Haimovici et al., 2017), it is likely that the observed age-related differences in BOLD signal variability might be confounded by such within-subject (state) variability. Therefore, future rsfMRI studies may benefit from obtaining arousal-related (e.g., self-report) measures and an explicit measurement of eye movements and eye opening/closure to account for the influence of arousal on the BOLD amplitude changes. Another option would be to combine EEG and fMRI simultaneously. Yet, resting state measures of EEG (Näpflin et al., 2007) and fMRI (Shehzad et al., 2009; Zuo et al., 2010) have been shown to be reliable within-individuals across time.

In our study, the computation of the source reconstructed rsEEG required the parcellation of the brain into relatively large anatomical ROIs. It could well be that the analysis with a higher spatial resolution (e.g., at the voxel-level) with individual head models may provide additional insights about brain signal variability.

Finally, while our study aimed at comparing analogous variability measures in EEG and fMRI, future research using rsEEG and rsfMRI in the same subjects would benefit from the addition of connectivity-based measures including graph theory-based (Yu et al., 2016) or sliding-window methods (Chang et al., 2013; Qin et al., 2019).

6. Conclusion

In this study, we report age and sex differences of brain signal variability obtained with rsfMRI and rsEEG from the same subjects. We demonstrate extensive age-related reduction of SD_{BOLD}, SD_{DELTA}, SD_{THETA}, and SD_{ALPHA} mainly in the DMN and the visual network, while a significant increase of SD_{BETA} was mainly seen in temporal brain regions. We could not demonstrate significant associations between SD_{BOLD} and $SD_{EEG.}$ Our findings indicate that measurements of BOLD and EEG signal variability, respectively, are likely to stem from different physiological origins and relate differentially to age and sex. While the two types of measurements are thus not interchangeable, it seems, however, plausible that both markers of brain variability may provide complementary information about the aging process.

7. Funding

This research did not receive any specific grant from funding agencies in the public, commercial, or not-for-profit sectors.

8. Acknowledgements

We gratefully acknowledge the Mind-Body- Emotion group at the Max Planck Institute for Human Cognitive and Brain Sciences.

9. References

Aanerud, J., Borghammer, P., Mallar Chakravarty, M., Vang, K., Rodell, A.B., Jónsdottir, K.Y., Møller, A., Ashkanian, M., Vafaee, M.S., Iversen, P., Johannsen, P., Gjedde, A., 2012. Brain energy metabolism and blood flow differences in healthy aging. J. Cereb. Blood Flow Metab. https://doi.org/10.1038/jcbfm.2012.18

Ances, B.M., Liang, C.L., Leontiev, O., Perthen, J.E., Fleisher, A.S., Lansing, A.E., Buxton, R.B., 2009. Effects of aging on cerebral blood flow, oxygen metabolism, and blood oxygenation level dependent responses to visual stimulation. Hum. Brain Mapp. 30, 1120–1132. https://doi.org/10.1002/hbm.20574

Andoh, J., Ferreira, M., Leppert, I.R., Matsushita, R., Pike, B., Zatorre, R.J., 2017. How restful is it with all that noise? Comparison of Interleaved silent steady state (ISSS) and conventional imaging in resting-state fMRI. Neuroimage 147, 726–735. https://doi.org/10.1016/j.neuroimage.2016.11.065

Andrews-Hanna, J.R., Smallwood, J., Spreng, R.N., 2014. The default network and self-generated thought: Component processes, dynamic control, and clinical relevance. Ann. N. Y. Acad. Sci. 1316, 29–52. https://doi.org/10.1111/nyas.12360

Armbruster-Genc, D.J.N., Ueltzhoffer, K., Fiebach, C.J., 2016. Brain Signal Variability Differentially Affects Cognitive Flexibility and Cognitive Stability. J. Neurosci. 36, 3978–3987. https://doi.org/10.1523/JNEUROSCI.2517-14.2016

Armitage, R., 1995. The distribution of EEG frequencies in REM and NREM sleep stages in healthy young adults. Sleep 18, 334–341. https://doi.org/10.1093/sleep/18.5.334

Aurlien, H., Gjerde, I.., Aarseth, J.., Eldøen, G., Karlsen, B., Skeidsvoll, H., Gilhus, N.., 2003. EEG background activity described by a large computerized database. Clin. Neurophysiol. 115, 665–673. https://doi.org/10.1016/j.clinph.2003.10.019

Avants, B.B., Tustison, N.J., Song, G., Cook, P.A., Klein, A., Gee, J.C., 2011. A reproducible evaluation of ANTs similarity metric performance in brain image registration. Neuroimage 54, 2033–2044. https://doi.org/10.1016/j.neuroimage.2010.09.025

Babayan, A., Erbey, M., Kumral, D., Reinelt, J.D., Reiter, A.M.F., Röbbig, J., Lina Schaare, H., Uhlig, M., Anwander, A., Bazin, P.L., Horstmann, A., Lampe, L., Nikulin, V. V., Okon-Singer, H., Preusser, S., Pampel, A., Rohr, C.S., Sacher, J., Thöne-Otto, A., Trapp, S., Nierhaus, T., Altmann, D., Arelin, K., Blöchl, M., Bongartz, E., Breig, P., Cesnaite, E., Chen, S., Cozatl, R., Czerwonatis, S., Dambrauskaite, G., Dreyer, M., Enders, J., Engelhardt, M., Fischer, M.M., Forschack, N., Golchert, J., Golz, L., Guran, C.A., Hedrich, S., Hentschel, N., Hoffmann, D.I., Huntenburg, J.M., Jost, R., Kosatschek, A., Kunzendorf, S., Lammers, H., Lauckner, M.E., Mahjoory, K., Kanaan, A.S., Mendes, N., Menger, R., Morino, E., Näthe, K., Neubauer, J., Noyan, H., Oligschläger, S., Panczyszyn-Trzewik, P., Poehlchen, D., Putzke, N., Roski, S., Schaller, M.C., Schieferbein, A., Schlaak, B., Schmidt, R., Gorgolewski, K.J., Schmidt, H.M., Schrimpf, A., Stasch, S., Voss, M., Wiedemann, A., Margulies, D.S., Gaebler, M., Villringer, A., 2019. Data descriptor: A mind-brain-body dataset of MRI, EEG, cognition, emotion, and peripheral physiology in young and old adults. Sci. Data 6, 180308. https://doi.org/10.1038/sdata.2018.308

Babiloni, C., Binetti, G., Cassarino, A., Dal Forno, G., Del Percio, C., Ferreri, F., Ferri, R., Frisoni, G., Galderisi, S., Hirata, K., Lanuzza, B., Miniussi, C., Mucci, A., Nobili, F., Rodriguez, G., Romani, G.L., Rossini, P.M., Forno, G.D., Percio, C. Del, Ferreri, F., Ferri, R., Frisoni, G., Galderisi, S., Hirata, K., Lanuzza, B., Miniussi, C., Mucci, A., Nobili, F., Rodriguez, G., Romani, G.L., Rossini, P.M., 2006. Sources of cortical rhythms in adults during physiological aging: A multicentric EEG study. Hum. Brain Mapp. 27, 162–172. https://doi.org/10.1002/hbm.20175

Babiloni, C., Carducci, F., Lizio, R., Vecchio, F., Baglieri, A., Bernardini, S., Cavedo, E., Bozzao, A., Buttinelli, C., Esposito, F., Giubilei, F., Guizzaro, A., Marino, S., Montella, P., Quattrocchi, C.C., Redolfi, A., Soricelli, A., Tedeschi, G., Ferri, R., Rossi-Fedele, G., Ursini, F., Scrascia, F., Vernieri, F., Pedersen, T.J., Hardemark, H.G., Rossini, P.M., Frisoni, G.B., 2013. Resting state cortical electroencephalographic rhythms are related to gray matter volume in subjects with mild cognitive impairment and Alzheimer’s disease. Hum. Brain Mapp. 34, 1427–1446. https://doi.org/10.1002/hbm.22005

Bazanova, O.M., Vernon, D., 2014. Interpreting EEG alpha activity. Neurosci. Biobehav. Rev. 44, 94–110. https://doi.org/10.1016/j.neubiorev.2013.05.007

Bazin, P.L., Weiss, M., Dinse, J., Schäfer, A., Trampel, R., Turner, R., 2014. A computational framework for ultra-high resolution cortical segmentation at 7 Tesla. Neuroimage 93, 201–209. https://doi.org/10.1016/j.neuroimage.2013.03.077

Behzadi, Y., Restom, K., Liau, J., Liu, T.T., 2007. A component based noise correction method (CompCor) for BOLD and perfusion based fMRI. Neuroimage 37, 90–101. https://doi.org/10.1016/j.neuroimage.2007.04.042

Bell, A.J., Sejnowski, T.J., 1995. An Information-Maximization Approach to Blind Separation and Blind Deconvolution. Neural Comput. 7, 1129–1159. https://doi.org/10.1162/neco.1995.7.6.1129

Benjamini, Y., Hochberg, Y., 1995. Controlling the False Discovery Rate : A Practical and Powerful Approach to Multiple Testing Author (s): Yoav Benjamini and Yosef Hochberg Source : Journal of the Royal Statistical Society . Series B (Methodological), Vol . 57 , No . 1 Published by : J. R. Stat. Soc. 57, 289–300.

Bijsterbosch, J., Harrison, S., Duff, E., Alfaro-Almagro, F., Woolrich, M., Smith, S., 2017. Investigations into within- and between-subject resting-state amplitude variations. Neuroimage 159, 57–69. https://doi.org/10.1016/j.neuroimage.2017.07.014

Birn, R.M., Murphy, K., Bandettini, P.A., 2008. The effect of respiration variations on independent component analysis results of resting state functional connectivity. Hum. Brain Mapp. 29, 740–

750. https://doi.org/10.1002/hbm.20577

Biswal, B.B., Mennes, M., Zuo, X.-N., 2010. Toward discovery science of human brain function. Proc. Natl. Acad. Sci. U. S. A. 107, 4734–4739. https://doi.org/10.1073/pnas.0911855107

Brenner, R.P., Ulrich, R.F., Reynolds, C.F., 1995. EEG spectral findings in healthy, elderly men and women - sex differences. Electroencephalogr. Clin. Neurophysiol. 94, 1–5. https://doi.org/10.1016/0013-4694(94)00234-C

Brookes, M.J., Woolrich, M., Luckhoo, H., Price, D., Hale, J.R., Stephenson, M.C., Barnes, G.R., Smith, S.M., Morris, P.G., 2011. Investigating the electrophysiological basis of resting state networks using magnetoencephalography. Proc. Natl. Acad. Sci. 108, 16783–16788. https://doi.org/10.1073/pnas.1112685108

Burgess, A., Gruzelier, J., 1993. Individual reliability of amplitude distribution in topographical mapping of EEG. Electroencephalogr. Clin. Neurophysiol. 86, 219–223. https://doi.org/10.1016/0013-4694(93)90101-Z

Caballero-Gaudes, C., Reynolds, R.C., 2017. Methods for cleaning the BOLD fMRI signal. Neuroimage 154, 128–149. https://doi.org/10.1016/j.neuroimage.2016.12.018

Cabeza, R., 2001. Cognitive neuroscience of aging: Contributions of functional neuroimaging. Scand. J. Psychol. 42, 277–286. https://doi.org/10.1111/1467-9450.00237

Cabeza, R., Albert, M., Belleville, S., Craik, F.I.M., Duarte, A., Grady, C.L., Lindenberger, U., Nyberg, L., Park, D.C., Reuter-Lorenz, P.A., Rugg, M.D., Steffener, J., Rajah, M.N., 2018. Maintenance, reserve and compensation: the cognitive neuroscience of healthy ageing. Nat. Rev. Neurosci. 19, 701–710. https://doi.org/10.1038/s41583-018-0068-2

Campbell, K.L., Grady, C.L., Ng, C., Hasher, L., 2012. Age differences in the frontoparietal cognitive control network: Implications for distractibility. Neuropsychologia 50, 2212–2223. https://doi.org/10.1016/j.neuropsychologia.2012.05.025

Carrier, J., Land, S., Buysse, D.J., Kupfer, D.J., Monk, T.H., 2001. The effects of age and gender on sleep EEG power spectral density in the middle years of life (ages 20-60 years old). Psychophysiology 38, 232–242. https://doi.org/10.1017/S0048577201991838

Chang, C., Cunningham, J.P., Glover, G.H., 2009. Influence of heart rate on the BOLD signal: The cardiac response function. Neuroimage 44, 857–869. https://doi.org/10.1016/j.neuroimage.2008.09.029

Chang, C., Leopold, D.A., Schölvinck, M.L., Mandelkow, H., Picchioni, D., Liu, X., Ye, F.Q., Turchi, J.N., Duyn, J.H., 2016. Tracking brain arousal fluctuations with fMRI. Proc. Natl. Acad. Sci. 113, 4518–4523. https://doi.org/10.1073/pnas.1520613113

Chang, C., Liu, Z., Chen, M.C., Liu, X., Duyn, J.H., 2013. EEG correlates of time-varying BOLD functional connectivity. Neuroimage 72, 227–236. https://doi.org/10.1016/j.neuroimage.2013.01.049

Cho, Z., Chung, S., Lim, D., Wong, E.K., 1998. Effects of the Acoustic Noise of the Gradient Systems on fMRI: Magn. Reson. Med. 39 331–335.

Cohen, M.X., 2017. Where Does EEG Come From and What Does It Mean? Trends Neurosci. 40, 208–218. https://doi.org/10.1016/j.tins.2017.02.004

Cox, R.W., 1996. AFNI: Software for Analysis and Visualization of Functional Magnetic Resonance Neuroimages. Comput. Biomed. Res. 29, 162–173. https://doi.org/10.1006/cbmr.1996.0014

D'Esposito, M., Deouell, L.Y., Gazzaley, A., 2003. Alterations in the BOLD fMRI signal with ageing and disease: a challenge for neuroimaging. Nat. Rev. Neurosci. 4, 863–872. https://doi.org/10.1038/nrn1246

Damoiseaux, J.S., 2017. Effects of aging on functional and structural brain connectivity. Neuroimage 160, 32–40. https://doi.org/10.1016/j.neuroimage.2017.01.077

Damoiseaux, J.S., Beckmann, C.F., Arigita, E.J.S., Barkhof, F., Scheltens, P., Stam, C.J., Smith, S.M., Rombouts, S.A.R.B., 2008. Reduced resting-state brain activity in the "default network" in normal aging. Cereb. Cortex 18, 1856–1864. https://doi.org/10.1093/cercor/bhm207

Das, S.R., Pluta, J., Mancuso, L., Kliot, D., Yushkevich, P.A., Wolk, D.A., 2015. Anterior and posterior MTL networks in aging and MCI. Neurobiol. Aging 36, S141–S150. https://doi.org/10.1016/j.neurobiolaging.2014.03.041

Deligianni, F., Centeno, M., Carmichael, D.W., Clayden, J.D., 2014. Relating resting-state fMRI and EEG whole-brain connectomes across frequency bands. Front. Neurosci. 8, 1–16. https://doi.org/10.3389/fnins.2014.00258

Delorme, A., Makeig, S., 2004. EEGLAB: an open sorce toolbox for analysis of single-trail EEG dynamics including independent component anlaysis. J. Neurosci. Methods 134, 9–21. https://doi.org/10.1016/j.jneumeth.2003.10.009

Desikan, R.S., Ségonne, F., Fischl, B., Quinn, B.T., Dickerson, B.C., Blacker, D., Buckner, R.L., Dale, A.M., Maguire, R.P., Hyman, B.T., Albert, M.S., Killiany, R.J., 2006. An automated labeling system for subdividing the human cerebral cortex on MRI scans into gyral based regions of interest. Neuroimage 31, 968–980. https://doi.org/10.1016/j.neuroimage.2006.01.021

Dierks, T., Jelic, V., Pascual-Marqui, R.D., Wahlund, L.O., Julin, P., Linden, D.E.J., Maurer, K., Winblad, B., Nordberg, A., 2000. Spatial pattern of cerebral glucose metabolism (PET) correlates with localization of intracerebral EEG-generators in Alzheimer's disease. Clin. Neurophysiol. 111, 1817–1824. https://doi.org/10.1016/S1388-2457(00)00427-2

Duffy, F.H., McAnulty, G.B., Albert, M.S., 1993. The pattern of age-related differences in electrophysiological activity of healthy males and females. Neurobiol. Aging 14, 73–84. https://doi.org/10.1016/0197-4580(93)90025-7

Dustman, R.E., Shearer, D.E., Emmerson, R.Y., 1999. Life-span changes in EEG spectral amplitude, amplitude variability and mean frequency. Clin. Neurophysiol. 110, 1399–1409. https://doi.org/10.1016/S1388-2457(99)00102-9

Dustman, R.E., Shearer, D.E., Emmerson, R.Y., 1993. EEG and event-related potentials in normal aging. Prog. Neurobiol. 41, 369–401. https://doi.org/10.1016/0301-0082(93)90005-D

Engel, A.K., Fries, P., 2010. Beta-band oscillations-signalling the status quo? Curr. Opin. Neurobiol. 20, 156–165. https://doi.org/10.1016/j.conb.2010.02.015

Failla, M., Grappiolo, A., Emanuelli, G., Vitale, G., Fraschini, N., Bigoni, M., Grieco, N., Denti, M., Giannattasio, C., Mancia, G., 1999. Sympathetic tone restrains arterial distensibility of healthy and atherosclerotic subjects. J. Hypertens. 17, 1117–1123. https://doi.org/10.1097/00004872-199917080-00011

Farkas, E., Luiten, P.G.M., 2001. Cerebral microvascular pathology in aging and Alzheimer's disease, Progress in Neurobiology. https://doi.org/10.1016/S0301-0082(00)00068-X

Fernández, A., Zuluaga, P., Abásolo, D., Gómez, C., Serra, A., Méndez, M.A., Hornero, R., 2012. Brain oscillatory complexity across the life span. Clin. Neurophysiol. 123, 2154–2162. https://doi.org/10.1016/j.clinph.2012.04.025

Fischl, B., 2012. FreeSurfer. Neuroimage 62, 774–781. https://doi.org/10.1016/j.neuroimage.2012.01.021

Friston, K.J., Williams, S., Howard, R., Frackowiak, R.S.J., Turner, R., 1996. Movement-related effects in fMRI time-series. Magn. Reson. Med. 35, 346–355. https://doi.org/10.1002/mrm.1910350312

Garrett, D.D., Kovacevic, N., McIntosh, A.R., Grady, C.L., 2013a. The modulation of BOLD variability between cognitive states varies by age and processing speed. Cereb. Cortex 23, 684–693. https://doi.org/10.1093/cercor/bhs055

Garrett, D.D., Lindenberger, U., Hoge, R.D., Gauthier, C.J., 2017. Age differences in brain signal variability are robust to multiple vascular controls. Sci. Rep. 7, 10149. https://doi.org/10.1038/s41598-017-09752-7

Garrett, D.D., Nagel, I.E., Preuschhof, C., Burzynska, A.Z., Marchner, J., Wiegert, S., Jungehülsing, G.J., Nyberg, L., Villringer, A., Li, S.-C., Heekeren, H.R., Bäckman, L., Lindenberger, U., 2015. Amphetamine modulates brain signal variability and working memory in younger and older adults. Proc. Natl. Acad. Sci. 112, 7593–7598. https://doi.org/10.1073/pnas.1504090112

Garrett, D.D., Samanez-Larkin, G.R., MacDonald, S.W.S., Lindenberger, U., McIntosh, A.R., Grady, C.L., 2013b. Moment-to-moment brain signal variability: A next frontier in human brain mapping? Neurosci. Biobehav. Rev. 37, 610–624. https://doi.org/10.1016/j.neubiorev.2013.02.015

Geerligs, L., Tsvetanov, K.A., Cam-CAN, Henson, R.N., 2017. Challenges in measuring individual differences in functional connectivity using fMRI: The case of healthy aging. Hum. Brain Mapp. 38, 4125–4156. https://doi.org/10.1002/hbm.23653

Golchert, J., Smallwood, J., Jefferies, E., Seli, P., Huntenburg, J.M., Liem, F., Lauckner, M.E., Oligschläger, S., Bernhardt, B.C., Villringer, A., Margulies, D.S., 2017. Individual variation in intentionality in the mind-wandering state is reflected in the integration of the default-mode, fronto-parietal, and limbic networks. Neuroimage 146, 226–235. https://doi.org/10.1016/j.neuroimage.2016.11.025

Goldman, R.I., Stern, J.M., Engel, J., Cohen, M.S., 2002. Simultaneous EEG and fMRI of the alpha rhythm. Neuroreport 13, 2487–2492. https://doi.org/10.1097/00001756-200212200-00022

Gonçalves, S.I., De Munck, J.C., Pouwels, P.J.W., Schoonhoven, R., Kuijer, J.P.A., Maurits, N.M., Hoogduin, J.M., Van Someren, E.J.W., Heethaar, R.M., Lopes Da Silva, F.H., 2006. Correlating the alpha rhythm to BOLD using simultaneous EEG/fMRI: Inter-subject variability. Neuroimage 30, 203–213. https://doi.org/10.1016/j.neuroimage.2005.09.062

Gong, G., He, Y., Evans, A.C., 2011. Brain connectivity: Gender makes a difference. Neuroscientist 17, 575–591. https://doi.org/10.1177/1073858410386492

Gorgolewski, K., Burns, C.D., Madison, C., Clark, D., Halchenko, Y.O., Waskom, M.L., Ghosh, S.S., 2011. Nipype: A Flexible, Lightweight and Extensible Neuroimaging Data Processing Framework in Python. Front. Neuroinform. 5, 13. https://doi.org/10.3389/fninf.2011.00013

Grady, C., 2012. The cognitive neuroscience of ageing. Nat. Rev. Neurosci. 13, 491–505. https://doi.org/10.1038/nrn3256

Grady, C.L., Garrett, D.D., 2018. Brain signal variability is modulated as a function of internal and external demand in younger and older adults. Neuroimage 169, 510–523. https://doi.org/10.1016/j.neuroimage.2017.12.031

Grady, C.L., Garrett, D.D., 2014. Understanding variability in the BOLD signal and why it matters for aging. Brain Imaging Behav. https://doi.org/10.1007/s11682-013-9253-0

Greicius, M.D., Srivastava, G., Reiss, A.L., Menon, V., 2004. Default-mode network activity distinguishes Alzheimer's disease from healthy aging: evidence from functional MRI. Proc. Natl. Acad. Sci. U. S. A. 101, 4637–42. https://doi.org/10.1073/pnas.0308627101

Gur, R.C., Gur, R.E., Obrist, W.D., Hungerbuhler, J.P., Younkin, D., Rosen, A.D., Skolnick, B.E., Reivich, M., 1982. Sex and handedness differences in cerebral blood flow during rest and cognitive activity. Science (80-.). 217, 659–661. https://doi.org/10.1126/science.7089587

Haimovici, A., Tagliazucchi, E., Balenzuela, P., Laufs, H., 2017. On wakefulness fluctuations as a source of BOLD functional connectivity dynamics. Sci. Rep. 7. https://doi.org/10.1038/s41598-017-06389-4

Hartikainen, P., Soininen, H., Partanen, J., Helkala, E.L., Riekkinen, P., 1992. Aging and spectral analysis of EEG in normal subjects: a link to memory and CSF AChE. Acta Neurol. Scand. 86, 148–155. https://doi.org/10.1111/j.1600-0404.1992.tb05057.x

Haufe, S., Ewald, A., 2016. A Simulation Framework for Benchmarking EEG-Based Brain Connectivity Estimation Methodologies. Brain Topogr. 1–18. https://doi.org/10.1007/s10548-016-0498-y

Hawkes, C.H., Prescott, R.J., 1973. EEG variation in healthy subjects. Electroencephalogr. Clin. Neurophysiol. 34, 197–199. https://doi.org/10.1016/0013-4694(73)90048-5

Huang, Y., Parra, L.C., Haufe, S., 2016. The New York Head—A precise standardized volume conductor model for EEG source localization and tES targeting. Neuroimage 140, 150–162. https://doi.org/10.1016/j.neuroimage.2015.12.019

Hudetz, A.G., Biswal, B.B., Shen, H., Lauer, K.K., Kampine, J.P., 1998. Spontaneous Fluctuations in Cerebral Oxygen Supply. Springer, Boston, MA, pp. 551–559. https://doi.org/10.1007/978-1-4615-4863-8_66

Immer, F.R., 1937. Correlation between Means and Standard Deviations in Field Experiments. J. Am. Stat. Assoc. 32, 525–531. https://doi.org/10.1080/01621459.1937.10502321

Jacobson, S.C., Blanchard, M., Connolly, C.C., Cannon, M., Garavan, H., 2011. An fMRI investigation of a novel analogue to the Trail-Making Test. Brain Cogn. 77, 60–70. https://doi.org/10.1016/j.bandc.2011.06.001

Jaušovec, N., Jaušovec, K., 2010. Resting brain activity: Differences between genders. Neuropsychologia 48, 3918–3925. https://doi.org/10.1016/j.neuropsychologia.2010.09.020

Jenkinson, M., Beckmann, C.F., Behrens, T.E.J., Woolrich, M.W., Smith, S.M., 2012. Fsl. Neuroimage 62, 782–790. https://doi.org/10.1016/j.neuroimage.2011.09.015

Jollife, I.T., Cadima, J., 2016. Principal component analysis: A review and recent developments. Philos. Trans. R. Soc. A Math. Phys. Eng. Sci. 374, 20150202. https://doi.org/10.1098/rsta.2015.0202

Jorge, J., Van der Zwaag, W., Figueiredo, P., 2014. EEG-fMRI integration for the study of human brain function. Neuroimage 102, 24–34. https://doi.org/10.1016/j.neuroimage.2013.05.114

Jurcak, V., Tsuzuki, D., Dan, I., 2007. 10/20, 10/10, and 10/5 systems revisited: Their validity as relative head-surface-based positioning systems. Neuroimage 34, 1600–1611. https://doi.org/10.1016/j.neuroimage.2006.09.024

Kielar, A., Deschamps, T., Chu, R.K.O., Jokel, R., Khatamian, Y.B., Chen, J.J., Meltzer, J.A., 2016. Identifying dysfunctional cortex: Dissociable effects of stroke and aging on resting state dynamics in MEG and fmri. Front. Aging Neurosci. 8. https://doi.org/10.3389/fnagi.2016.00040

Klimesch, W., 1999. EEG alpha and theta oscillations reflect cognitive and memory performance: A review and analysis. Brain Res. Rev. 29, 169–195. https://doi.org/10.1016/S0165-0173(98)00056-3

Labrenz, F., Ferri, F., Wrede, K., Forsting, M., Schedlowski, M., Engler, H., Elsenbruch, S., Benson, S., Costantini, M., 2018. Altered temporal variance and functional connectivity of BOLD signal is associated with state anxiety during acute systemic inflammation. Neuroimage 184, 916–924. https://doi.org/10.1016/j.neuroimage.2018.09.056

Latta, F., Leproult, R., Tasali, E., Hofmann, E., Van Cauter, E., 2005. Sex differences in delta and alpha EEG activities in healthy older adults. Sleep 28, 1525–1534. https://doi.org/10.1093/sleep/28.12.1525

Laufs, H., Kleinschmidt, A., Holt, J.L., Elfont, R., Krams, M., Paul, J.S., Krakow, K., 2006. Where the

BOLD signal goes when alpha EEG leaves. Neuroimage 31, 1408–1418. https://doi.org/10.1016/j.neuroimage.2006.02.002

Laufs, H., Krakow, K., Sterzer, P., Eger, E., Beyerle, A., Kleinschmidt, A., 2003. Electroencephalographic signatures of attentional and cognitive default modes in spontaneous brain activity fluctuations at rest 100.

Lipsitz, L.A., Goldberger, A.L., 1992. Loss of 'Complexity' and Aging: Potential Applications of Fractals and Chaos Theory to Senescence. JAMA J. Am. Med. Assoc. 267, 1806–1809. https://doi.org/10.1001/jama.1992.03480130122036

Liu, P., Hebrank, A.C., Rodrigue, K.M., Kennedy, K.M., Section, J., Park, D.C., Lu, H., 2013. Age-related differences in memory-encoding fMRI responses after accounting for decline in vascular reactivity. Neuroimage 78, 415–425. https://doi.org/10.1016/j.neuroimage.2013.04.053

Liu, T.T., 2013. Neurovascular factors in resting-state functional MRI. Neuroimage 80, 339–348. https://doi.org/10.1016/j.neuroimage.2013.04.071

Logothetis, N.K., 2008. What we can do and what we cannot do with fMRI. Nature 453, 869–878. https://doi.org/10.1038/nature06976

Logothetis, N.K., Wandell, B.A., 2004. Interpreting the BOLD Signal. Annu. Rev. Physiol. 66, 735–769. https://doi.org/10.1146/annurev.physiol.66.082602.092845

Lopes Da Silva, F.H., Pijn, J.P., Velis, D., Nijssen, P.C.G., 1997. Alpha rhythms: Noise, dynamics and models. Int. J. Psychophysiol. 26, 237–249. https://doi.org/10.1016/S0167-8760(97)00767-8

Lopez-Larson, M.P., Anderson, J.S., Ferguson, M.A., Yurgelun-Todd, D., 2011. Local brain connectivity and associations with gender and age. Dev. Cogn. Neurosci. 1, 187–197. https://doi.org/10.1016/j.dcn.2010.10.001

Ma, Y., Shaik, M.A., Kozberg, M.G., Kim, S.H., Portes, J.P., Timerman, D., Hillman, E.M.C., 2016. Resting-state hemodynamics are spatiotemporally coupled to synchronized and symmetric neural activity in excitatory neurons. Proc. Natl. Acad. Sci. 113, E8463–E8471. https://doi.org/10.1073/pnas.1525369113

Malone, I.B., Leung, K.K., Clegg, S., Barnes, J., Whitwell, J.L., Ashburner, J., Fox, N.C., Ridgway, G.R., 2015. Accurate automatic estimation of total intracranial volume: A nuisance variable with less nuisance. Neuroimage 104, 366–372. https://doi.org/10.1016/j.neuroimage.2014.09.034

Maltez, J., Hyllienmark, L., Nikulin, V. V., Brismar, T., 2004. Time course and variability of power in different frequency bands of EEG during resting conditions. Neurophysiol. Clin. 34, 195–202. https://doi.org/10.1016/j.neucli.2004.09.003

Mantini, D., Perrucci, M.G., Del Gratta, C., Romani, G.L., Corbetta, M., 2007. Electrophysiological signatures of resting state networks in the human brain. Proc. Natl. Acad. Sci. 104, 13170–13175. https://doi.org/10.1073/pnas.0700668104

Margulies, D.S., Ghosh, S.S., Goulas, A., Falkiewicz, M., Huntenburg, J.M., Langs, G., Bezgin, G., Eickhoff, S.B., Castellanos, F.X., Petrides, M., Jefferies, E., Smallwood, J., 2016. Situating the default-mode network along a principal gradient of macroscale cortical organization. Proc. Natl. Acad. Sci. 113, 12574–12579. https://doi.org/10.1073/pnas.1608282113

Martin, J., Friston, K.J., Colebatch, J.G., Frackowiak, R.S.J., Unit, M.R.C.C., Hospital, H., 1991. Decreases in Regional Cerebral Blood Flow with Normal Aging 684–689.

Mateo, C., Knutsen, P.M., Tsai, P.S., Shih, A.Y., Kleinfeld, D., 2017. Entrainment of Arteriole Vasomotor Fluctuations by Neural Activity Is a Basis of Blood-Oxygenation-Level-Dependent “Resting-State” Connectivity. Neuron 96, 936-948.e3. https://doi.org/10.1016/j.neuron.2017.10.012

Matsuura, M., Yamamoto, K., Fukuzawa, H., Okubo, Y., Uesugi, H., Moriiwa, M., Kojima, T., Shimazono, Y., 1985. Age development and sex differences of various EEG elements in healthy children and adults - Quantification by a computerized waveform recognition method. Electroencephalogr. Clin. Neurophysiol. 60, 394–406. https://doi.org/10.1016/0013-4694(85)91013-2

McBride, J.C., Zhao, X., Munro, N.B., Smith, C.D., Jicha, G.A., Hively, L., Broster, L.S., Schmitt, F.A., Kryscio, R.J., Jiang, Y., 2014. Spectral and complexity analysis of scalp EEG characteristics for mild cognitive impairment and early Alzheimer’s disease. Comput. Methods Programs Biomed. 114, 153–163. https://doi.org/10.1016/j.cmpb.2014.01.019

McDonald, J.H., 2014. Handbook of Biological Statistics. Sparky House Publ. 180–185.

Meunier, D., Achard, S., Morcom, A., Bullmore, E., 2009. Age-related changes in modular organization of human brain functional networks. Neuroimage 44, 715–723. https://doi.org/10.1016/j.neuroimage.2008.09.062

Meyer, M.C., Janssen, R.J., Van Oort, E.S.B., Beckmann, C.F., Barth, M., 2013. The Quest for EEG Power Band Correlation with ICA Derived fMRI Resting State Networks. Front. Hum. Neurosci. 7, 315. https://doi.org/10.3389/fnhum.2013.00315

Moosmann, M., Ritter, P., Krastel, I., Brink, A., Thees, S., Blankenburg, F., Taskin, B., Obrig, H., Villringer, A., 2003. Correlates of alpha rhythm in functional magnetic resonance imaging and near infrared spectroscopy. Neuroimage 20, 145–158. https://doi.org/10.1016/S1053-8119(03)00344-6

Moretti, D. V., Paternicò, D., Binetti, G., Zanetti, O., Frisoni, G.B., 2012. EEG markers are associated to gray matter changes in thalamus and basal ganglia in subjects with mild cognitive impairment. Neuroimage 60, 489–496. https://doi.org/10.1016/j.neuroimage.2011.11.086

Murayama, Y., Bieβmann, F., Logothetis, N.K., Oeltermann, A., Müller, K.-R., Meinecke, F.C., Augath, M., 2010. Relationship between neural and hemodynamic signals during spontaneous activity studied with temporal kernel CCA. Magn. Reson. Imaging 28, 1095–1103. https://doi.org/10.1016/j.mri.2009.12.016

Murphy, K., Birn, R.M., Bandettini, P.A., 2013. Resting-state fMRI confounds and cleanup. Neuroimage 80, 349–359. https://doi.org/10.1016/j.neuroimage.2013.04.001

Näpflin, M., Wildi, M., Sarnthein, J., 2007. Test-retest reliability of resting EEG spectra validates a statistical signature of persons. Clin. Neurophysiol. 118, 2519–2524. https://doi.org/10.1016/j.clinph.2007.07.022

Nguyen, L.H., Holmes, S., 2019. Ten quick tips for effective dimensionality reduction. PLOS Comput. Biol. 15, e1006907. https://doi.org/10.1371/journal.pcbi.1006907

Niessing, J., Ebisch, B., Schmidt, K.E., Niessing, M., Singer, W., Galuske, R.A.W., 2005. Neuroscience: Hemodynamic signals correlate tightly with synchronized gamma oscillations. Science (80-.). 309, 948–951. https://doi.org/10.1126/science.1110948

Nir, Y., Hasson, U., Levy, I., Yeshurun, Y., Malach, R., 2006. Widespread functional connectivity and fMRI fluctuations in human visual cortex in the absence of visual stimulation. Neuroimage 30, 1313–1324. https://doi.org/10.1016/j.neuroimage.2005.11.018

Nomi, J.S., Bolt, T.S., Ezie, C.E.C., Uddin, L.Q., Heller, A.S., 2017. Moment-to-Moment BOLD Signal Variability Reflects Regional Changes in Neural Flexibility across the Lifespan. J. Neurosci. 37, 5539–5548. https://doi.org/10.1523/JNEUROSCI.3408-16.2017

Nomi, J.S., Schettini, E., Voorhies, W., Bolt, T.S., Heller, A.S., Uddin, L.Q., 2018. Resting-State Brain Signal Variability in Prefrontal Cortex Is Associated With ADHD Symptom Severity in Children. Front. Hum. Neurosci. 12, 90. https://doi.org/10.3389/fnhum.2018.00090

Nunez, P.L., Srinivasan, R., Fields, R.D., 2015. EEG functional connectivity, axon delays and white matter disease. Clin. Neurophysiol. 126, 110–120. https://doi.org/10.1016/j.clinph.2014.04.003

Oken, B.S., Chiappa, K.H., 1988. Short-term variability in EEG frequency analysis. Electroencephalogr. Clin. Neurophysiol. 69, 191–198. https://doi.org/10.1016/0013-4694(88)90128-9

Petersen, S.E., Savalia, N.K., Chan, M.Y., Park, D.C., Wig, G.S., 2014. Decreased segregation of brain systems across the healthy adult lifespan. Proc. Natl. Acad. Sci. 111, E4997–E5006. https://doi.org/10.1073/pnas.1415122111

Qin, Y., Jiang, S., Zhang, Q., Dong, L., Jia, X., He, H., Yao, Y., Yang, H., Zhang, T., Luo, C., Yao, D., 2019. BOLD-fMRI activity informed by network variation of scalp EEG in juvenile myoclonic epilepsy. NeuroImage Clin. 22, 101759. https://doi.org/10.1016/j.nicl.2019.101759

Quandt, F., Bönstrup, M., Schulz, R., Timmermann, J.E., Zimerman, M., Nolte, G., Hummel, F.C., 2016. Spectral variability in the aged brain during fine motor control. Front. Aging Neurosci. 8. https://doi.org/10.3389/fnagi.2016.00305

Raichle, M.E., 2015. The Brain's Default Mode Network. Annu. Rev. Neurosci. 38, 433–447. https://doi.org/10.1146/annurev-neuro-071013-014030

Reitan, R.M., 1955. Certain differential effects of left and right cerebral lesions in human adults. J Comp Physiol Psychol 48, 474–477.

Reitan, R.M., Wolfson, D., 1995. Category Test and Trail Making Test as Measures of Frontal Lobe Functions. Clin. Neuropsychol. 9, 50–56. https://doi.org/10.1080/13854049508402057

Rice, J.K., Rorden, C., Little, J.S., Parra, L.C., 2013. Subject position affects EEG magnitudes. Neuroimage 64, 476–484. https://doi.org/10.1016/j.neuroimage.2012.09.041

Ritter, P., Moosmann, M., Villringer, A., 2009. Rolandic alpha and beta EEG rhythms' strengths are inversely related to fMRI-BOLD signal in primary somatosensory and motor cortex. Hum. Brain Mapp. 30, 1168–1187. https://doi.org/10.1002/hbm.20585

Ritter, P., Villringer, A., 2006. Simultaneous EEG-fMRI. Neurosci. Biobehav. Rev. 30, 823–838. https://doi.org/10.1016/j.neubiorev.2006.06.008

Rodriguez, G., Warkentin, S., Risberg, J., Rosadini, G., 1988. Sex differences in regional cerebral blood flow. J. Cereb. Blood Flow Metab. 8, 783–789. https://doi.org/10.1038/jcbfm.1988.133

Rokem, a, Trumpis, M., Perez, F., 2009. Nitime: time-series analysis for neuroimaging data. Proc. 8th Python Sci. Conf. (SciPy 2009) 1–8.

Rosenblum, M., Pikovsky, A., Kurths, J., Schäfer, C., Tass, P.A., 2001. Phase synchronization: From theory to data analysis. Handb. Biol. Phys. 4, 279–321. https://doi.org/10.1016/S1383-8121(01)80012-9

Rossiter, H.E., Davis, E.M., Clark, E. V., Boudrias, M.H., Ward, N.S., 2014. Beta oscillations reflect changes in motor cortex inhibition in healthy ageing. Neuroimage 91, 360–365. https://doi.org/10.1016/j.neuroimage.2014.01.012

Ruigrok, A.N.V., Salimi-Khorshidi, G., Lai, M.C., Baron-Cohen, S., Lombardo, M. V., Tait, R.J., Suckling, J., 2014. A meta-analysis of sex differences in human brain structure. Neurosci. Biobehav. Rev. 39, 34–50. https://doi.org/10.1016/j.neubiorev.2013.12.004

Sacher, J., Neumann, J., Okon-Singer, H., Gotowiec, S., Villringer, A., 2013. Sexual dimorphism in the human brain: Evidence from neuroimaging. Magn. Reson. Imaging 31, 366–375. https://doi.org/10.1016/j.mri.2012.06.007

Scheeringa, R., Fries, P., Petersson, K.M., Oostenveld, R., Grothe, I., Norris, D.G., Hagoort, P., Bastiaansen, M.C.M., 2011. Neuronal Dynamics Underlying High- and Low-Frequency EEG Oscillations Contribute Independently to the Human BOLD Signal. Neuron 69, 572–583. https://doi.org/10.1016/j.neuron.2010.11.044

Seaquist, E.R., Chen, W., Benedict, L.E., Ugurbil, K., Kwag, J.H., Zhu, X.H., Nelson, C.A., 2007. Insulin reduces the BOLD response but is without effect on the VEP during presentation of a visual task in humans. J. Cereb. Blood Flow Metab. 27, 154–160. https://doi.org/10.1038/sj.jcbfm.9600316

Shehzad, Z., Kelly, A.M.C., Reiss, P.T., Gee, D.G., Gotimer, K., Uddin, L.Q., Lee, S.H., Margulies, D.S., Roy, A.K., Biswal, B.B., Petkova, E., Castellanos, F.X., Milham, M.P., 2009. The Resting Brain: Unconstrained yet Reliable. Cereb. Cortex 19, 2209–2229. https://doi.org/10.1093/cercor/bhn256

Sleimen-Malkoun, R., Perdikis, D., Muller, V., Blanc, J.-L., Huys, R., Temprado, J.-J., Jirsa, V.K., 2015. Brain Dynamics of Aging: Multiscale Variability of EEG Signals at Rest and during an

Auditory Oddball Task. eNeuro 2. https://doi.org/10.1523/ENEURO.0067-14.2015

Smits, F.M., Porcaro, C., Cottone, C., Cancelli, A., Rossini, P.M., Tecchio, F., 2016. Electroencephalographic fractal dimension in healthy ageing and Alzheimer's disease. PLoS One 11, 1–16. https://doi.org/10.1371/journal.pone.0149587

Speelman, C.P., McGann, M., 2013. How mean is the mean? Front. Psychol. 4, 1–12. https://doi.org/10.3389/fpsyg.2013.00451

Spreng, R.N., Sepulcre, J., Turner, G.R., Stevens, W.D., Schacter, D.L., 2013. Intrinsic Architecture Underlying the Relations among the Default, Dorsal Attention, and Frontoparietal Control Networks of the Human Brain. J. Cogn. Neurosci. 25, 74–86. https://doi.org/10.1162/jocn_a_00281

Steriade, M., 2006. Grouping of brain rhythms in corticothalamic systems. Neuroscience 137, 1087–1106. https://doi.org/10.1016/j.neuroscience.2005.10.029

Stomrud, E., Hansson, O., Minthon, L., Blennow, K., Rosén, I., Londos, E., 2010. Slowing of EEG correlates with CSF biomarkers and reduced cognitive speed in elderly with normal cognition over 4 years. Neurobiol. Aging 31, 215–223. https://doi.org/10.1016/j.neurobiolaging.2008.03.025

Tagliazucchi, E., Laufs, H., 2014. Decoding Wakefulness Levels from Typical fMRI Resting-State Data Reveals Reliable Drifts between Wakefulness and Sleep. Neuron 82, 695–708. https://doi.org/10.1016/j.neuron.2014.03.020

Thompson, G.J., 2018. Neural and metabolic basis of dynamic resting state fMRI. Neuroimage 180, 448–462. https://doi.org/10.1016/j.neuroimage.2017.09.010

Tibshirani, R., 2011. Regression shrinkage and selection via the lasso: a retrospective. J. R. Stat. Soc. Ser. B (Statistical Methodol. 73, 273–282. https://doi.org/10.1111/j.1467-9868.2011.00771.x

Tomasi, D., Volkow, N.D., 2012. Aging and functional brain networks. Mol. Psychiatry 17, 549–558. https://doi.org/10.1038/mp.2011.81

Tsvetanov, K.A., Henson, R.N.A., Tyler, L.K., Davis, S.W., Shafto, M.A., Taylor, J.R., Williams, N., Cam-Can, Rowe, J.B., 2015. The effect of ageing on fMRI: Correction for the confounding effects of vascular reactivity evaluated by joint fMRI and MEG in 335 adults. Hum. Brain Mapp. 36, 2248–2269. https://doi.org/10.1002/hbm.22768

Vaillancourt, D.E., Newell, K.M., 2002. Changing complexity in human behavior and physiology through aging and disease. Neurobiol Aging 23, 1–11. https://doi.org/10.1016/S0197-4580(02)00052-0

Valdés-Hernández, P.A., Ojeda-González, A., Martínez-Montes, E., Lage-Castellanos, A., Virués-Alba, T., Valdés-Urrutia, L., Valdes-Sosa, P.A., 2010. White matter architecture rather than cortical surface area correlates with the EEG alpha rhythm. Neuroimage 49, 2328–2339. https://doi.org/10.1016/j.neuroimage.2009.10.030

Veldhuizen, R.J., Jonkman, E.J., Poortvliet, D.C.J., 1993. Sex differences in age regression parameters of healthy adults-normative data and practical implications. Electroencephalogr. Clin. Neurophysiol. 86, 377–384. https://doi.org/10.1016/0013-4694(93)90133-G

Villringer, A., Dirnagl, U., 1995. Coupling of brain activity and cerebral blood flow: basis of functional neuroimaging. Cerebrovasc. Brain Metab. Rev. 7, 240—276.

Vlahou, E.L., Thurm, F., Kolassa, I.-T., Schlee, W., 2015. Resting-state slow wave power, healthy aging and cognitive performance. Sci. Rep. 4, 5101. https://doi.org/10.1038/srep05101

Wang, R., Foniok, T., Wamsteeker, J.I., Qiao, M., Tomanek, B., Vivanco, R.A., Tuor, U.I., 2006. Transient blood pressure changes affect the functional magnetic resonance imaging detection of cerebral activation. Neuroimage 31, 1–11. https://doi.org/10.1016/j.neuroimage.2005.12.004

Wheeler, R.E., 2016. lmPerm: Permutation tests for linear models. http://CRAN.R-project.org/package=lmPerm. 24 p.

Witten, D.M., Tibshirani, R., Hastie, T., 2009. A penalized matrix decomposition, with applications to sparse principal components and canonical correlation analysis. Biostatistics 10, 515–534. https://doi.org/10.1093/biostatistics/kxp008

Wong, C.W., Olafsson, V., Tal, O., Liu, T.T., 2013. The amplitude of the resting-state fMRI global signal is related to EEG vigilance measures. Neuroimage 83, 983–990. https://doi.org/10.1016/j.neuroimage.2013.07.057

Yan, C.G., Craddock, R.C., Zuo, X.N., Zang, Y.F., Milham, M.P., 2013. Standardizing the intrinsic brain: Towards robust measurement of inter-individual variation in 1000 functional connectomes. Neuroimage 80, 246–262. https://doi.org/10.1016/j.neuroimage.2013.04.081

Yang, A.C., Huang, C.C., Yeh, H.L., Liu, M.E., Hong, C.J., Tu, P.C., Chen, J.F., Huang, N.E., Peng, C.K., Lin, C.P., Tsai, S.J., 2013. Complexity of spontaneous BOLD activity in default mode network is correlated with cognitive function in normal male elderly: A multiscale entropy analysis. Neurobiol. Aging 34, 428–438. https://doi.org/10.1016/j.neurobiolaging.2012.05.004

Yu, Q., Wu, L., Bridwell, D.A., Erhardt, E.B., Du, Y., He, H., Chen, J., Liu, P., Sui, J., Pearlson, G., Calhoun, V.D., 2016. Building an EEG-fMRI Multi-Modal Brain Graph: A Concurrent EEG-fMRI Study. Front. Hum. Neurosci. 10, 1–17. https://doi.org/10.3389/fnhum.2016.00476

Zakzanis, K., Mraz, R., Graham, S., 2005. An fMRI study of the trail making test. Neuropsychologia.

Zappasodi, F., Marzetti, L., Olejarczyk, E., Tecchio, F., Pizzella, V., 2015. Age-related changes in electroencephalographic signal complexity. PLoS One 10, 1–13. https://doi.org/10.1371/journal.pone.0141995

Zappasodi, F., Pasqualetti, P., Tombini, M., Ercolani, M., Pizzella, V., Rossini, P.M., Tecchio, F., 2006. Hand cortical representation at rest and during activation: Gender and age effects in the two hemispheres. Clin. Neurophysiol. 117, 1518–1528. https://doi.org/10.1016/j.clinph.2006.03.016

Ziegler, E., Chellappa, S.L., Gaggioni, G., Ly, J.Q.M., Vandewalle, G., André, E., Geuzaine, C., Phillips, C., 2014. A finite-element reciprocity solution for EEG forward modeling with realistic individual head models. Neuroimage 103, 542–551. https://doi.org/10.1016/j.neuroimage.2014.08.056

Zöller, D., Schaer, M., Scariati, E., Padula, M.C., Eliez, S., Van De Ville, D., 2017. Disentangling resting-state BOLD variability and PCC functional connectivity in 22q11.2 deletion syndrome. Neuroimage 149, 85–97. https://doi.org/10.1016/j.neuroimage.2017.01.064

Zuo, X.N., Di Martino, A., Kelly, C., Shehzad, Z.E., Gee, D.G., Klein, D.F., Castellanos, F.X., Biswal, B.B., Milham, M.P., 2010. The oscillating brain: Complex and reliable. Neuroimage 49, 1432–1445. https://doi.org/10.1016/j.neuroimage.2009.09.037

10. Supplementary Material

Supplementary Figure 1. Flowchart of selecting participants from the Mind-Brain-Body study.

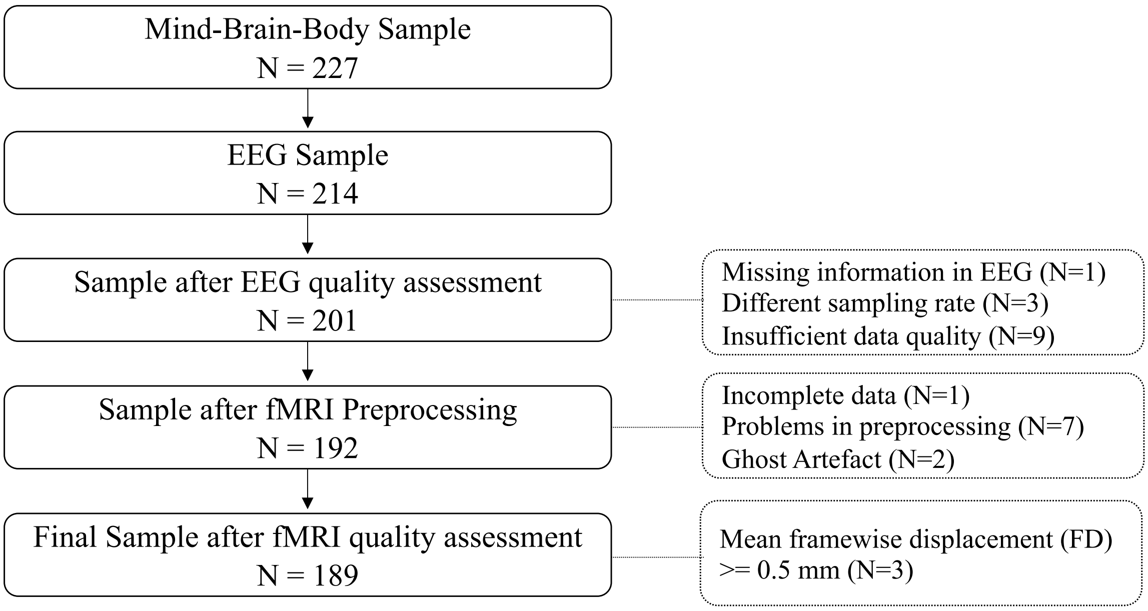

Supplementary Figure 2. Spatial maps of mean SD_{BOLD} and SD_{EEG} for younger adults (N=135). We computed the mean SD_{BOLD} and SD_{EEG} by I) log-transforming the SD values, II) averaging separately for younger and older subjects, and III) then back-transforming the values (McDonald, 2014).

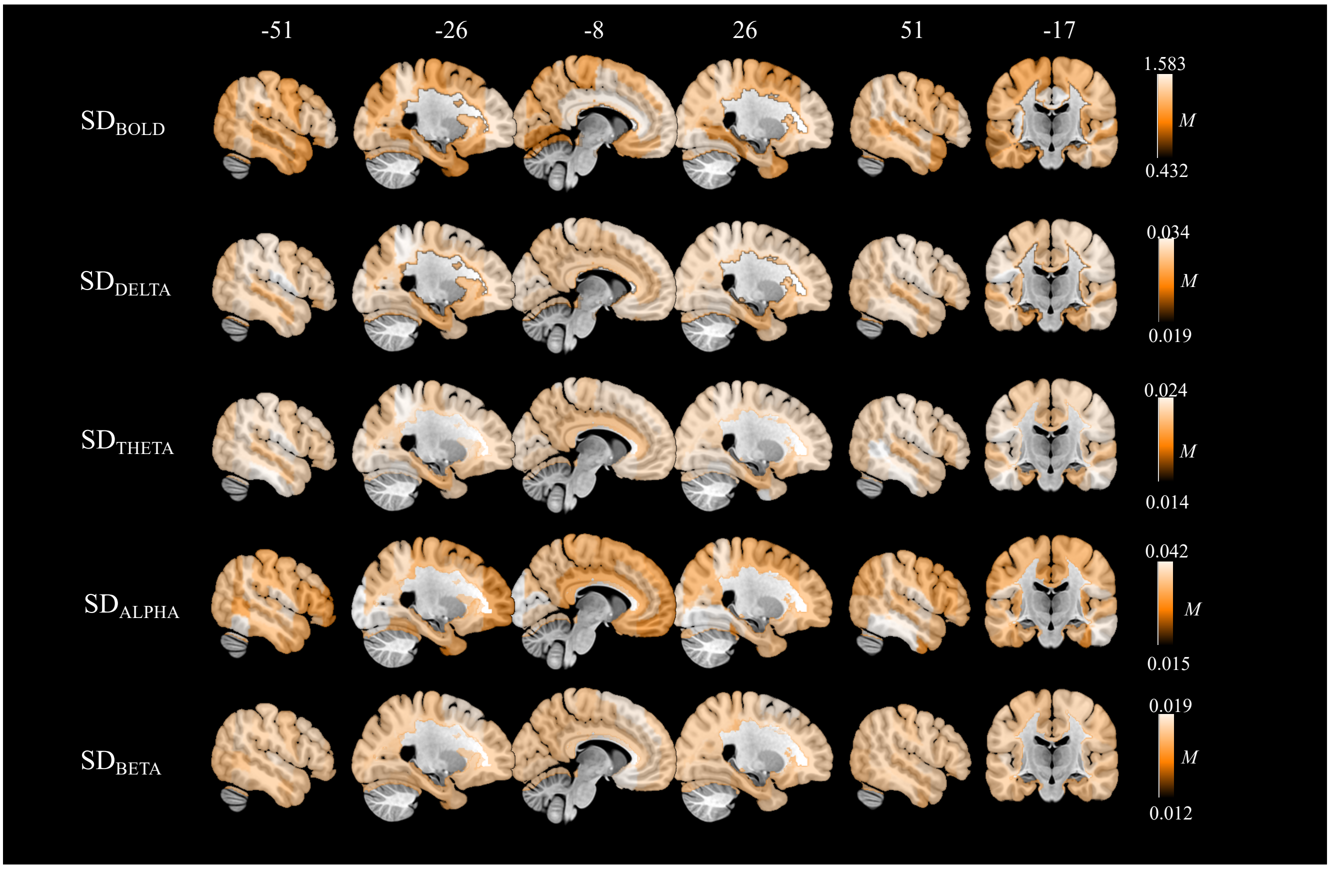

Supplementary Figure 3. Spatial maps of mean SD_{BOLD} and SD_{EEG} for older adults (N=54). We computed the mean SD_{BOLD} and SD_{EEG} by I) log-transforming the SD values, II) averaging separately for younger and older subjects, and III) then back-transforming the values (McDonald, 2014).

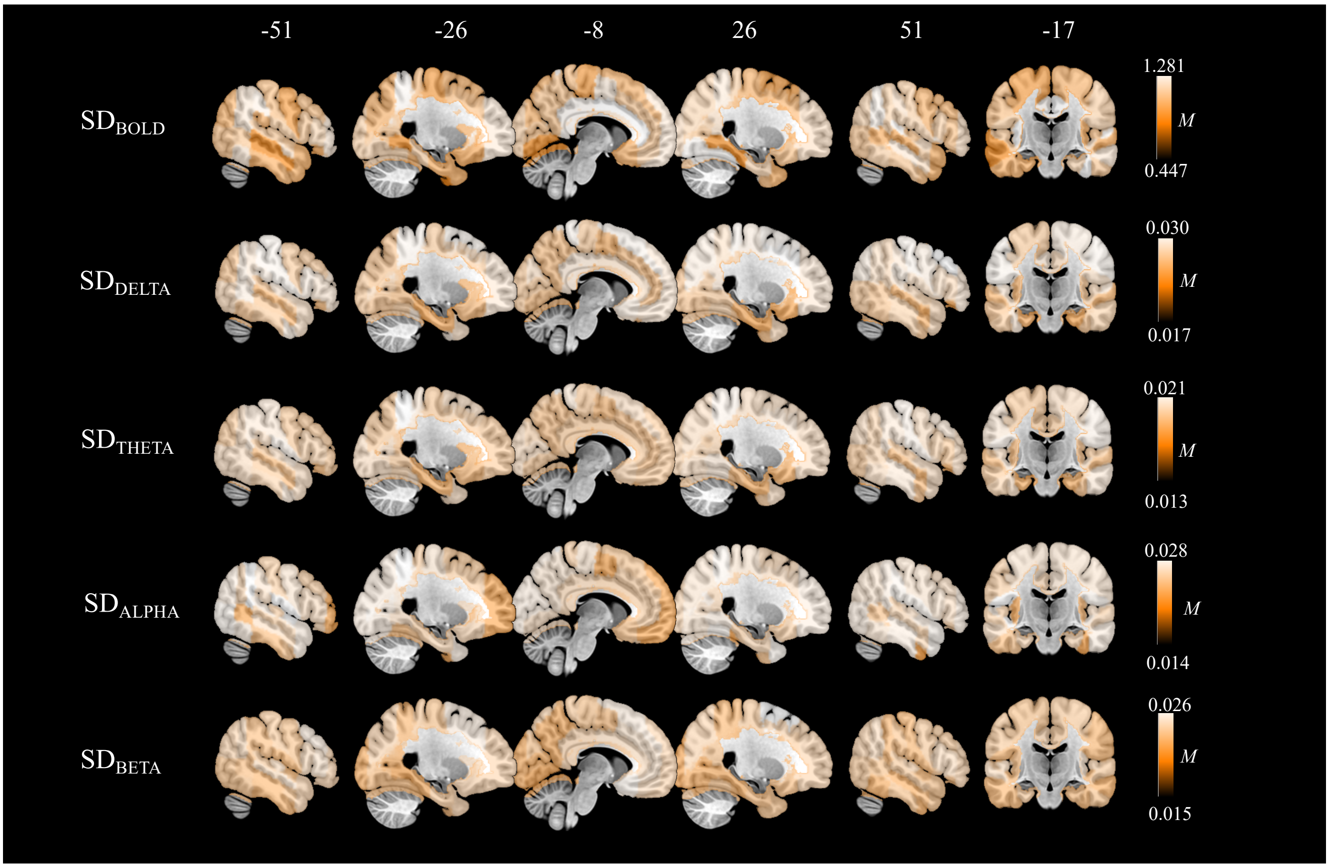

Supplementary Figure 4. Graphical distribution of the F-values for significant effects of age group or sex. The nonparametric ANCOVAs with SD_{BOLD} as dependent variable demonstrated that there was a significant main effect of age group in 72 ROIs, while no significant effect of sex was observed. We further found significant main effects of age group in all EEG frequency bands: SD_{DELTA} in 14 ROIs (F-values: 12.57–20.94), SD_{THETA} in 16 ROIs (F-values: 13.16–40.30), SD_{ALPHA} in 20 ROIs (F-values: 12.69–20.12), and SD_{BETA} in 69 ROIs (F-values: 12.50–21.61). There were also significant main effects of sex in all frequency bands: SD_{DELTA} in 21 ROIs (F-values: 13.24–26.63), SD_{THETA} in 74 ROIs (F-values: 12.68–30.06), SD_{ALPHA} in 4 ROIs (F-values: 12.88–16.51), and SD_{BETA} in 69 ROIs (F-values: 12.54–35.72).

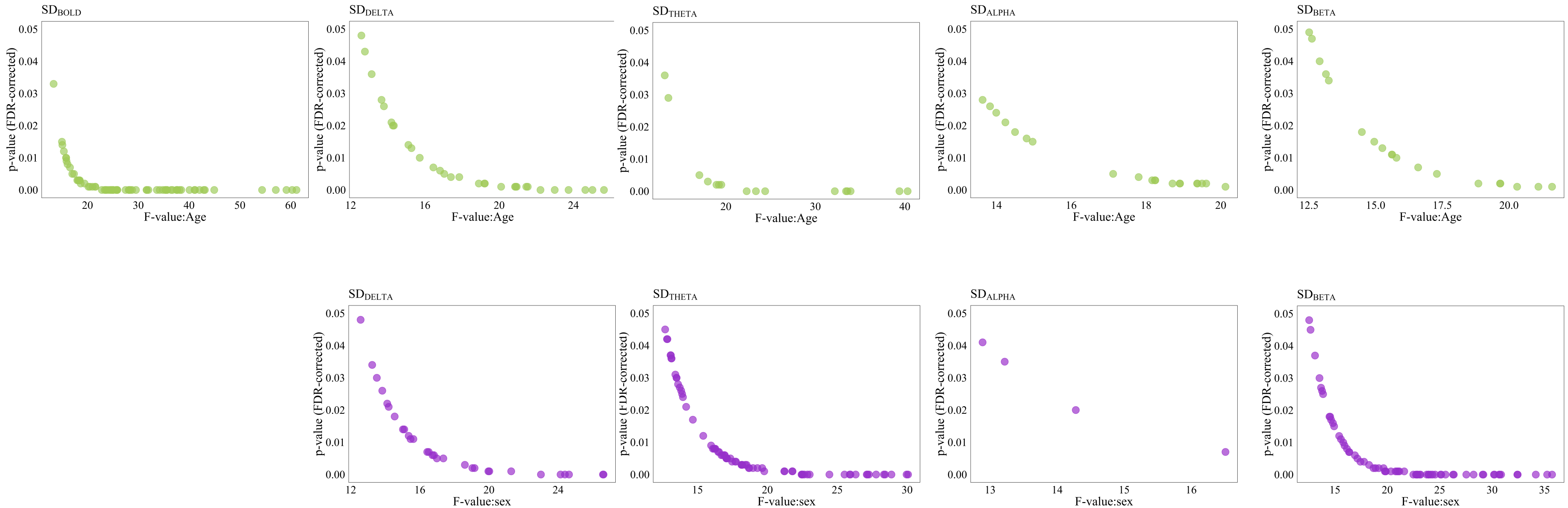

Supplementary Table 1: Table showing the mean (*M*) values of the SD_{BOLD} and SD_{EEG} for younger (N=135) and older (N=54) adults, respectively.

	SD_{BOLD}		SD_{DELTA}		SD_{THETA}		SD_{ALPHA}		SD_{BETA}	
ROI	**Young**	**Old**	**Young**	**Old**	**Young**	**Old**	**Young**	**Old**	**Young**	**Old**
Left Frontal Pole	1.336	1.085	0.028	0.027	0.019	0.016	0.015	0.016	0.014	0.021
Right Frontal Pole	1.304	1.029	0.027	0.027	0.020	0.018	0.026	0.026	0.015	0.021
Left Insular Cortex	1.583	1.213	0.023	0.019	0.021	0.014	0.022	0.016	0.014	0.018
Right Insular Cortex	0.845	0.728	0.024	0.022	0.019	0.015	0.021	0.018	0.016	0.023
Left Superior Frontal Gyrus	0.883	0.767	0.030	0.029	0.021	0.018	0.021	0.021	0.018	0.024
Right Superior Frontal Gyrus	0.735	0.651	0.028	0.029	0.021	0.018	0.022	0.023	0.018	0.026
Left Middle Frontal Gyrus	0.981	0.848	0.024	0.023	0.020	0.016	0.029	0.022	0.016	0.024
Right Middle Frontal Gyrus	0.868	0.789	0.029	0.030	0.020	0.019	0.021	0.024	0.015	0.020
Left Inferior Frontal Gyrus, pars triangularis	1.170	0.992	0.026	0.027	0.017	0.017	0.019	0.024	0.015	0.023
Right Inferior Frontal Gyrus, pars triangularis	0.977	0.848	0.024	0.025	0.016	0.016	0.020	0.024	0.014	0.022
Left Inferior Frontal Gyrus, pars opercularis	1.162	0.905	0.027	0.028	0.018	0.017	0.020	0.024	0.015	0.022
Right Inferior Frontal Gyrus, pars opercularis	1.077	0.949	0.025	0.026	0.017	0.017	0.021	0.025	0.014	0.022
Left Precentral Gyrus	0.710	0.646	0.024	0.023	0.017	0.016	0.024	0.025	0.013	0.019
Right Precentral Gyrus	0.875	0.766	0.028	0.028	0.019	0.018	0.022	0.025	0.015	0.020
Left Temporal Pole	0.733	0.741	0.027	0.026	0.019	0.018	0.023	0.026	0.014	0.021
Right Temporal Pole	0.761	0.746	0.027	0.025	0.019	0.018	0.027	0.027	0.015	0.019
Left Superior Temporal Gyrus, anterior division	1.089	1.028	0.022	0.021	0.017	0.015	0.029	0.023	0.015	0.023
Right Superior Temporal Gyrus, anterior division	1.041	0.921	0.020	0.017	0.016	0.013	0.030	0.022	0.013	0.020
Left Superior Temporal Gyrus, posterior division	0.485	0.447	0.019	0.019	0.015	0.014	0.025	0.022	0.014	0.022
Right Superior Temporal Gyrus, posterior division	0.748	0.693	0.020	0.019	0.015	0.014	0.026	0.023	0.013	0.020
Left Middle Temporal Gyrus, anterior division	0.457	0.507	0.020	0.019	0.015	0.014	0.026	0.023	0.012	0.019
Right Middle Temporal Gyrus, anterior division	1.255	1.019	0.024	0.019	0.017	0.014	0.033	0.023	0.013	0.017
Left Middle Temporal Gyrus, posterior division	0.432	0.458	0.026	0.022	0.019	0.016	0.029	0.024	0.014	0.017
Right Middle Temporal Gyrus, posterior division	1.148	1.078	0.029	0.024	0.021	0.019	0.038	0.026	0.014	0.016

Left Middle Temporal Gyrus, temporooccipital part	1.009	0.888	0.027	0.028	0.020	0.018	0.017	0.016	0.012	0.018
Right Middle Temporal Gyrus, temporooccipital part	0.776	0.720	0.026	0.022	0.024	0.017	0.029	0.020	0.015	0.019
Left Inferior Temporal Gyrus, anterior division	0.819	0.773	0.028	0.028	0.022	0.019	0.022	0.020	0.013	0.017
Right Inferior Temporal Gyrus, anterior division	0.982	0.821	0.024	0.022	0.020	0.015	0.017	0.014	0.012	0.016
Left Inferior Temporal Gyrus, posterior division	0.886	0.737	0.026	0.023	0.023	0.017	0.025	0.019	0.014	0.017
Right Inferior Temporal Gyrus, posterior division	1.052	0.891	0.030	0.024	0.023	0.019	0.040	0.026	0.015	0.019
Left Inferior Temporal Gyrus, temporooccipital part	1.224	1.080	0.029	0.022	0.021	0.018	0.040	0.026	0.015	0.019
Right Inferior Temporal Gyrus, temporooccipital part	1.052	0.947	0.029	0.022	0.021	0.018	0.041	0.025	0.014	0.016
Left Postcentral Gyrus	0.940	0.845	0.030	0.029	0.021	0.019	0.021	0.022	0.015	0.020
Right Postcentral Gyrus	1.089	0.946	0.030	0.029	0.021	0.020	0.026	0.025	0.013	0.017
Left Superior Parietal Lobule	1.309	1.174	0.033	0.029	0.023	0.021	0.033	0.028	0.014	0.017
Right Superior Parietal Lobule	1.282	1.093	0.030	0.026	0.021	0.020	0.035	0.027	0.014	0.017
Left Supramarginal Gyrus, anterior division	1.291	1.127	0.029	0.029	0.020	0.019	0.023	0.025	0.014	0.018
Right Supramarginal Gyrus, anterior division	1.213	1.051	0.030	0.027	0.021	0.019	0.027	0.027	0.014	0.019
Left Supramarginal Gyrus, posterior division	1.148	1.092	0.030	0.027	0.021	0.019	0.032	0.028	0.015	0.018
Right Supramarginal Gyrus, posterior division	1.100	0.968	0.029	0.025	0.021	0.019	0.032	0.026	0.015	0.017
Left Angular Gyrus	1.230	1.076	0.028	0.028	0.021	0.018	0.023	0.023	0.016	0.022
Right Angular Gyrus	1.323	1.149	0.025	0.026	0.018	0.017	0.024	0.025	0.015	0.022
Left Lateral Occipital Cortex, superior division	0.811	0.765	0.023	0.022	0.017	0.016	0.028	0.026	0.014	0.021
Right Lateral Occipital Cortex, superior division	1.072	0.981	0.027	0.028	0.019	0.018	0.022	0.025	0.014	0.021
Left Lateral Occipital Cortex, inferior division	0.890	0.861	0.026	0.025	0.019	0.018	0.027	0.027	0.013	0.019
Right Lateral Occipital Cortex, inferior division	1.100	0.892	0.024	0.023	0.018	0.016	0.027	0.026	0.013	0.020
Left Intracalcarine Cortex	1.072	0.863	0.030	0.023	0.021	0.018	0.041	0.026	0.014	0.016
Right Intracalcarine Cortex	0.885	0.893	0.028	0.023	0.020	0.017	0.034	0.024	0.014	0.015
Left Frontal Medial Cortex	0.946	0.945	0.029	0.027	0.019	0.016	0.017	0.016	0.016	0.022
Right Frontal Medial Cortex	1.349	1.063	0.027	0.026	0.020	0.017	0.028	0.024	0.015	0.021
Left Juxtapositional Lobule Cortex (formerly Supplementary Motor Cortex)	1.380	1.102	0.023	0.019	0.020	0.014	0.022	0.016	0.014	0.018

Right Juxtapositional Lobule Cortex (formerly Supplementary Motor Cortex)	0.925	0.784	0.024	0.020	0.019	0.014	0.023	0.018	0.017	0.023
Left Subcallosal Cortex	0.880	0.762	0.030	0.028	0.021	0.017	0.023	0.020	0.019	0.025
Right Subcallosal Cortex	0.984	0.846	0.028	0.027	0.021	0.017	0.024	0.021	0.019	0.025
Left Paracingulate Gyrus	1.251	0.902	0.023	0.021	0.019	0.015	0.029	0.022	0.016	0.023
Right Paracingulate Gyrus	0.942	0.822	0.029	0.028	0.019	0.018	0.021	0.022	0.015	0.021
Left Cingulate Gyrus, anterior division	1.487	1.213	0.024	0.026	0.015	0.016	0.020	0.022	0.014	0.022
Right Cingulate Gyrus, anterior division	1.459	1.201	0.023	0.024	0.015	0.016	0.022	0.024	0.013	0.020
Left Cingulate Gyrus, posterior division	1.412	1.163	0.025	0.027	0.016	0.016	0.020	0.023	0.014	0.021
Right Cingulate Gyrus, posterior division	1.579	1.281	0.024	0.025	0.016	0.016	0.023	0.025	0.014	0.020
Left Precuneous Cortex	0.978	0.878	0.024	0.021	0.017	0.015	0.029	0.025	0.013	0.016
Right Precuneous Cortex	1.120	1.041	0.027	0.027	0.018	0.017	0.022	0.023	0.014	0.019
Left Cuneal Cortex	0.793	0.764	0.027	0.026	0.018	0.017	0.027	0.026	0.014	0.019
Right Cuneal Cortex	0.894	0.837	0.028	0.024	0.020	0.017	0.033	0.027	0.015	0.017
Left Frontal Orbital Cortex	0.813	0.702	0.021	0.020	0.017	0.014	0.029	0.023	0.014	0.021
Right Frontal Orbital Cortex	1.166	0.850	0.021	0.017	0.016	0.013	0.030	0.022	0.013	0.018
Left Parahippocampal Gyrus, anterior division	0.853	0.733	0.019	0.018	0.014	0.013	0.027	0.023	0.013	0.020
Right Parahippocampal Gyrus, anterior division	1.129	0.975	0.020	0.017	0.015	0.013	0.029	0.023	0.013	0.018
Left Parahippocampal Gyrus, posterior division	1.101	0.943	0.021	0.017	0.016	0.013	0.030	0.022	0.013	0.016
Right Parahippocampal Gyrus, posterior division	0.459	0.455	0.024	0.018	0.018	0.014	0.035	0.022	0.013	0.016
Left Lingual Gyrus	0.550	0.554	0.027	0.021	0.019	0.016	0.034	0.024	0.015	0.015
Right Lingual Gyrus	0.558	0.544	0.030	0.023	0.021	0.019	0.041	0.026	0.015	0.016
Left Temporal Fusiform Cortex, anterior division	0.524	0.507	0.027	0.028	0.020	0.018	0.017	0.017	0.012	0.018
Right Temporal Fusiform Cortex, anterior division	0.929	0.807	0.026	0.021	0.024	0.016	0.029	0.020	0.015	0.019
Left Temporal Fusiform Cortex, posterior division	0.870	0.763	0.028	0.027	0.022	0.018	0.022	0.020	0.013	0.017
Right Temporal Fusiform Cortex, posterior division	1.387	1.244	0.024	0.022	0.020	0.015	0.017	0.015	0.013	0.017
Left Temporal Occipital Fusiform Cortex	1.258	0.961	0.027	0.023	0.023	0.017	0.025	0.019	0.014	0.018
Right Temporal Occipital Fusiform Cortex	1.367	1.187	0.031	0.024	0.023	0.019	0.040	0.027	0.015	0.019

Left Occipital Fusiform Gyrus	1.182	0.974	0.029	0.022	0.022	0.018	0.041	0.026	0.015	0.018
Right Occipital Fusiform Gyrus	1.416	1.169	0.029	0.022	0.021	0.018	0.042	0.025	0.015	0.016
Left Frontal Operculum Cortex	1.039	0.953	0.030	0.029	0.021	0.019	0.022	0.021	0.016	0.022
Right Frontal Operculum Cortex	1.299	1.207	0.031	0.028	0.021	0.019	0.027	0.025	0.014	0.018
Left Central Opercular Cortex	1.012	0.930	0.034	0.029	0.023	0.020	0.036	0.028	0.015	0.017
Right Central Opercular Cortex	1.032	0.976	0.031	0.026	0.022	0.020	0.037	0.027	0.015	0.017
Left Parietal Operculum Cortex	0.812	0.750	0.029	0.028	0.019	0.018	0.024	0.024	0.014	0.018
Right Parietal Operculum Cortex	1.072	0.988	0.030	0.028	0.021	0.019	0.031	0.027	0.015	0.018
Left Planum Polare	0.923	0.866	0.031	0.026	0.022	0.019	0.037	0.028	0.016	0.017
Right Planum Polare	1.339	1.024	0.029	0.024	0.021	0.018	0.036	0.026	0.016	0.017
Left Heschl's Gyrus (includes H1 and H2)	0.971	0.901	0.028	0.027	0.021	0.018	0.025	0.022	0.017	0.022
Right Heschl's Gyrus (includes H1 and H2)	0.917	0.841	0.024	0.025	0.017	0.016	0.026	0.024	0.014	0.021
Left Planum Temporale	0.994	0.912	0.024	0.022	0.017	0.016	0.032	0.026	0.014	0.020
Right Planum Temporale	1.429	1.176	0.026	0.027	0.017	0.016	0.023	0.022	0.014	0.020
Left Supracalcarine Cortex	1.340	1.098	0.027	0.026	0.019	0.018	0.030	0.027	0.013	0.018
Right Supracalcarine Cortex	1.135	0.953	0.024	0.023	0.018	0.016	0.030	0.026	0.013	0.019
Left Occipital Pole	1.180	0.954	0.030	0.023	0.021	0.018	0.042	0.026	0.014	0.016
Right Occipital Pole	1.284	1.025	0.028	0.022	0.019	0.017	0.036	0.023	0.014	0.015

Supplementary Table 2: Table showing the F-values for main effect of age group for BOLD signal variability (SD_{BOLD}). Statistical significance was determined using nonparametric ANCOVAs corrected for multiple comparisons by false discovery rates (FDR; Benjamini and Hochberg, 1995). The nonparametric ANCOVAs with SD_{BOLD} as dependent variable demonstrated that there was a significant main effect of age group in 72 ROIs, while no significant effect of sex was observed.

ROI	**F-value: age**
Left.Angular.Gyrus	20.9868
Left.Central.Opercular.Cortex	15.7773
Left.Cingulate.Gyrus..anterior.division	37.6699
Left.Cingulate.Gyrus..posterior.division	24.6328
Left.Cuneal.Cortex	20.4775
Left.Frontal.Medial.Cortex	16.5504
Left.Frontal.Orbital.Cortex	59.1622
Left.Frontal.Pole	27.4942
Left.Heschls.Gyrus..includes.H1.and.H2.	15.867
Left.Inferior.Frontal.Gyrus..pars.opercularis	42.0627
Left.Inferior.Frontal.Gyrus..pars.triangularis	17.0069
Left.Inferior.Temporal.Gyrus..posterior.division	28.2274
Left.Insular.Cortex	38.1285
Left.Intracalcarine.Cortex	34.2193
Left.Juxtapositional.Lobule.Cortex..formerly.Supplementary.Motor.Cortex.	40.0826
Left.Middle.Frontal.Gyrus	35.6619
Left.Middle.Temporal.Gyrus..temporooccipital.part	24.0403
Left.Occipital.Fusiform.Gyrus	35.3288
Left.Occipital.Pole	43.1077
Left.Paracingulate.Gyrus	54.3683
Left.Parahippocampal.Gyrus..anterior.division	60.2925
Left.Parahippocampal.Gyrus..posterior.division	38.4558

Left.Parietal.Operculum.Cortex	25.0314
Left.Postcentral.Gyrus	29.5352
Left.Precuneous.Cortex	28.1132
Left.Subcallosal.Cortex	35.3522
Left.Superior.Frontal.Gyrus	16.076
Left.Superior.Temporal.Gyrus..posterior.division	19.4259
Left.Supracalcarine.Cortex	25.8525
Left.Supramarginal.Gyrus..anterior.division	15.3458
Left.Temporal.Fusiform.Cortex..anterior.division	17.3434
Left.Temporal.Fusiform.Cortex..posterior.division	37.6047
Left.Temporal.Occipital.Fusiform.Cortex	41.0751
Right.Angular.Gyrus	22.823
Right.Cingulate.Gyrus..anterior.division	35.6207
Right.Cingulate.Gyrus..posterior.division	28.4509
Right.Cuneal.Cortex	25.6256
Right.Frontal.Medial.Cortex	44.9473
Right.Frontal.Orbital.Cortex	61.1423
Right.Frontal.Pole	36.7283
Right.Inferior.Frontal.Gyrus..pars.opercularis	14.9685
Right.Inferior.Frontal.Gyrus..pars.triangularis	15.799
Right.Inferior.Temporal.Gyrus..anterior.division	21.551
Right.Inferior.Temporal.Gyrus..posterior.division	15.0549
Right.Insular.Cortex	18.3847
Right.Intracalcarine.Cortex	13.3254
Right.Juxtapositional.Lobule.Cortex..formerly.Supplementary.Motor.Cortex.	36.4605
Right.Lateral.Occipital.Cortex..inferior.division	33.6556
Right.Lateral.Occipital.Cortex..superior.division	21.5155
Right.Lingual.Gyrus	25.0696

Right.Middle.Temporal.Gyrus..anterior.division	42.8831
Right.Occipital.Fusiform.Gyrus	31.6213
Right.Occipital.Pole	31.9927
Right.Paracingulate.Gyrus	34.8449
Right.Parahippocampal.Gyrus..anterior.division	37.5431
Right.Parietal.Operculum.Cortex	18.2991
Right.Planum.Polare	57.0714
Right.Planum.Temporale	25.7173
Right.Postcentral.Gyrus	20.1925
Right.Precentral.Gyrus	18.1681
Right.Precuneous.Cortex	24.8254
Right.Subcallosal.Cortex	41.1512
Right.Superior.Frontal.Gyrus	25.8665
Right.Superior.Parietal.Lobule	23.6064
Right.Superior.Temporal.Gyrus..anterior.division	17.9951
Right.Superior.Temporal.Gyrus..posterior.division	18.4805
Right.Supracalcarine.Cortex	28.7788
Right.Supramarginal.Gyrus..anterior.division	18.6616
Right.Supramarginal.Gyrus..posterior.division	23.6768
Right.Temporal.Fusiform.Cortex..anterior.division	23.371
Right.Temporal.Fusiform.Cortex..posterior.division	24.4233
Right.Temporal.Occipital.Fusiform.Cortex	31.6812

Supplementary Table 3: Table showing the F-values for the main effect of age group for EEG signal variability (1-3 Hz, SD_{DELTA}). Statistical significance was determined using nonparametric ANCOVAs corrected for multiple comparisons by false discovery rates (FDR; Benjamini and Hochberg, 1995). The nonparametric ANCOVAs with SD_{DELTA} as dependent variable demonstrated that there was a significant main effect of age group in 14 ROIs, and sex in in 20 ROIs.

ROI	**F-value: age**	**ROI**	**F-value: sex**
Left.Cingulate.Gyrus..posterior.division	17.041	Left.Cuneal.Cortex	15.463
Left.Cuneal.Cortex	20.8528	Left.Intracalcarine.Cortex	20.018
Left.Intracalcarine.Cortex	12.579	Left.Lingual.Gyrus	13.828
Left.Juxtapositional.Lobule.Cortex..formerly.Supplementary.Motor.Cortex.	13.1327	Left.Parietal.Operculum.Cortex	13.243
Left.Lateral.Occipital.Cortex..superior.division	15.2747	Left.Supracalcarine.Cortex	21.285
Left.Precuneous.Cortex	19.2268	Right.Cuneal.Cortex	17.36
Left.Supracalcarine.Cortex	16.815	Right.Heschls.Gyrus..includes.H1.and.H2.	15.627
Right.Cingulate.Gyrus..posterior.division	17.85	Right.Inferior.Temporal.Gyrus..posterior.division	16.731
Right.Cuneal.Cortex	20.1038	Right.Inferior.Temporal.Gyrus..temporooccipital.part	26.594
Right.Intracalcarine.Cortex	15.1102	Right.Intracalcarine.Cortex	26.625
Right.Juxtapositional.Lobule.Cortex..formerly.Supplementary.Motor.Cortex.	13.7918	Right.Lateral.Occipital.Cortex..inferior.division	24.394
Right.Lateral.Occipital.Cortex..superior.division	19.2019	Right.Lingual.Gyrus	19.964
Right.Precuneous.Cortex	20.9403	Right.Middle.Temporal.Gyrus..temporooccipital.part	24.628
Right.Supracalcarine.Cortex	17.4001	Right.Occipital.Fusiform.Gyrus	19.042
		Right.Occipital.Pole	14.198
		Right.Parahippocampal.Gyrus..posterior.division	15.023
		Right.Parietal.Operculum.Cortex	15.099
		Right.Planum.Temporale	16.428
		Right.Supracalcarine.Cortex	24.14
		Right.Temporal.Fusiform.Cortex..posterior.division	16.515
		Right.Temporal.Occipital.Fusiform.Cortex	23.004

Supplementary Table 4: Table showing the F-values for the main effect of age group for EEG signal variability (4-7 Hz, SD_{THETA}). Statistical significance was determined using nonparametric ANCOVAs corrected for multiple comparisons by false discovery rates (FDR; Benjamini and Hochberg, 1995). The nonparametric ANCOVAs with SD_{THETA} as dependent variable demonstrated that there was a significant main effect of age group in 16 ROIs, and sex in in 74 ROIs.

ROI	F-value: age	ROI	F-value: sex
Left.Cingulate.Gyrus..anterior.division	33.5753	Left.Angular.Gyrus	18.207
Left.Cingulate.Gyrus..posterior.division	19.2188	Left.Central.Opercular.Cortex	13.609
Left.Juxtapositional.Lobule.Cortex..formerly.Supplementary.Motor.Cortex.	39.3985	Left.Cingulate.Gyrus..anterior.division	13.504
Left.Middle.Frontal.Gyrus	24.3858	Left.Cingulate.Gyrus..posterior.division	17.748
Left.Paracingulate.Gyrus	22.3193	Left.Cuneal.Cortex	22.505
Left.Precentral.Gyrus	17.0336	Left.Frontal.Orbital.Cortex	13.146
Left.Precuneous.Cortex	13.1632	Left.Frontal.Pole	16.278
Left.Superior.Frontal.Gyrus	33.9343	Left.Inferior.Frontal.Gyrus..pars.opercularis	12.817
Right.Cingulate.Gyrus..anterior.division	32.1706	Left.Inferior.Temporal.Gyrus..posterior.division	13.732
Right.Cingulate.Gyrus..posterior.division	18.9454	Left.Inferior.Temporal.Gyrus..temporooccipital.part	16.711
Right.Juxtapositional.Lobule.Cortex..formerly.Supplementary.Motor.Cortex.	40.3098	Left.Intracalcarine.Cortex	27.158
Right.Middle.Frontal.Gyrus	23.3526	Left.Juxtapositional.Lobule.Cortex..formerly.Supplementary.Motor.Cortex.	13.129
Right.Paracingulate.Gyrus	19.4883	Left.Lateral.Occipital.Cortex..inferior.division	16.541
Right.Precentral.Gyrus	17.9796	Left.Lateral.Occipital.Cortex..superior.division	13.959
Right.Superior.Frontal.Gyrus	33.4244	Left.Lingual.Gyrus	22.478
Right.Superior.Parietal.Lobule	13.5708	Left.Middle.Temporal.Gyrus..temporooccipital.part	16.103
		Left.Occipital.Fusiform.Gyrus	18.143
		Left.Occipital.Pole	18.184
		Left.Parahippocampal.Gyrus..posterior.division	14.667

Left.Parietal.Operculum.Cortex	21.209
Left.Planum.Temporale	18.513
Left.Postcentral.Gyrus	16.801
Left.Precentral.Gyrus	16.951
Left.Precuneous.Cortex	17.475
Left.Subcallosal.Cortex	13.415
Left.Supracalcarine.Cortex	27.108
Left.Supramarginal.Gyrus..anterior.division	22.636
Left.Supramarginal.Gyrus..posterior.division	18.42
Left.Temporal.Fusiform.Cortex..posterior.division	12.846
Left.Temporal.Occipital.Fusiform.Cortex	18.695
Right.Angular.Gyrus	17.082
Right.Central.Opercular.Cortex	23.027
Right.Cingulate.Gyrus..anterior.division	13.094
Right.Cingulate.Gyrus..posterior.division	17.068
Right.Cuneal.Cortex	22.446
Right.Frontal.Operculum.Cortex	25.517
Right.Frontal.Orbital.Cortex	17.066
Right.Frontal.Pole	12.686
Right.Heschls.Gyrus..includes.H1.and.H2.	16.19
Right.Inferior.Frontal.Gyrus..pars.opercularis	25.941
Right.Inferior.Frontal.Gyrus..pars.triangularis	24.437
Right.Inferior.Temporal.Gyrus..anterior.division	19.63
Right.Inferior.Temporal.Gyrus..posterior.division	22.865
Right.Inferior.Temporal.Gyrus..temporooccipital.part	28.425
Right.Insular.Cortex	22.486
Right.Intracalcarine.Cortex	29.957
Right.Juxtapositional.Lobule.Cortex..formerly.Supplementary.Motor	13.499

Right.Lateral.Occipital.Cortex..inferior.division	30.063
Right.Lateral.Occipital.Cortex..superior.division	13.899
Right.Lingual.Gyrus	25.891
Right.Middle.Frontal.Gyrus	18.676
Right.Middle.Temporal.Gyrus..anterior.division	13.832
Right.Middle.Temporal.Gyrus..posterior.division	21.779
Right.Middle.Temporal.Gyrus..temporooccipital.part	28.874
Right.Occipital.Fusiform.Gyrus	27.265
Right.Occipital.Pole	28.335
Right.Parahippocampal.Gyrus..anterior.division	15.973
Right.Parahippocampal.Gyrus..posterior.division	17.709
Right.Parietal.Operculum.Cortex	16.92
Right.Planum.Polare	17.124
Right.Planum.Temporale	17.351
Right.Postcentral.Gyrus	18.97
Right.Precentral.Gyrus	21.799
Right.Precuneous.Cortex	16.222
Right.Subcallosal.Cortex	14.188
Right.Superior.Temporal.Gyrus..anterior.division	13.072
Right.Superior.Temporal.Gyrus..posterior.division	19.288
Right.Supracalcarine.Cortex	27.779
Right.Supramarginal.Gyrus..anterior.division	19.774
Right.Supramarginal.Gyrus..posterior.division	15.411
Right.Temporal.Fusiform.Cortex..anterior.division	18.158
Right.Temporal.Fusiform.Cortex..posterior.division	21.228
Right.Temporal.Occipital.Fusiform.Cortex	26.317
Right.Temporal.Pole	16.482

Supplementary Table 5: Table showing the F-values for the main effect of age group for EEG signal variability (8-12 Hz, SD_{ALPHA}). Statistical significance was determined using nonparametric ANCOVAs corrected for multiple comparisons by false discovery rates (FDR; Benjamini and Hochberg, 1995). The nonparametric ANCOVAs with SD_{ALPHA} as dependent variable demonstrated that there was a significant main effect of age group in 20 ROIs, and sex in in 4 ROIs.

ROI	**F-value: age**	**ROI**	**F-value: sex**
Left.Cingulate.Gyrus..anterior.division	14.2391	Left.Frontal.Pole	16.512
Left.Cingulate.Gyrus..posterior.division	18.9122	Right.Frontal.Orbital.Cortex	13.217
Left.Cuneal.Cortex	19.5004	Right.Inferior.Frontal.Gyrus..pars.triangularis	14.278
Left.Intracalcarine.Cortex	13.9943	Right.Temporal.Pole	12.887
Left.Juxtapositional.Lobule.Cortex..formerly.Supplementary.Motor.Cortex.	18.2498		
Left.Lateral.Occipital.Cortex..superior.division	14.8073		
Left.Occipital.Pole	13.6297		
Left.Precuneous.Cortex	18.1658		
Left.Supracalcarine.Cortex	18.7095		
Right.Cingulate.Gyrus..anterior.division	14.9683		
Right.Cingulate.Gyrus..posterior.division	19.3745		
Right.Cuneal.Cortex	20.1265		
Right.Intracalcarine.Cortex	17.8042		
Right.Juxtapositional.Lobule.Cortex..formerly.Supplementary.Motor.Cortex.	18.9006		
Right.Lateral.Occipital.Cortex..superior.division	18.2382		
Right.Occipital.Pole	17.1219		
Right.Precuneous.Cortex	19.3677		
Right.Superior.Frontal.Gyrus	14.4975		
Right.Superior.Parietal.Lobule	13.8287		
Right.Supracalcarine.Cortex	19.6116		

Supplementary Table 6: Table showing the F-values for the main effect of age group for EEG signal variability (15-25 Hz, SD_{BETA}). Statistical significance was determined using nonparametric ANCOVAs corrected for multiple comparisons by false discovery rates (FDR; Benjamini and Hochberg, 1995). The nonparametric ANCOVA analyses with SD_{BETA} as dependent variable demonstrated that there was a significant main effect of age group in 19 ROIs, and sex in 69 ROIs.

ROI	**F-value: age**	**ROI**	**F-value: sex**
Left.Central.Opercular.Cortex	16.5945	Left.Angular.Gyrus	23.069
Left.Heschls.Gyrus..includes.H1.and.H2.	20.3049	Left.Cingulate.Gyrus..anterior.division	12.198
Left.Inferior.Temporal.Gyrus..posterior.division	15.6087	Left.Cingulate.Gyrus..posterior.division	23.953
Left.Insular.Cortex	12.903	Left.Cuneal.Cortex	29.101
Left.Middle.Temporal.Gyrus..posterior.division	13.2449	Left.Frontal.Medial.Cortex	20.926
Left.Parietal.Operculum.Cortex	21.6143	Left.Frontal.Operculum.Cortex	12.549
Left.Planum.Temporale	21.1029	Left.Frontal.Orbital.Cortex	22.762
Left.Superior.Temporal.Gyrus..posterior.division	14.4852	Left.Frontal.Pole	19.186
Left.Supramarginal.Gyrus..anterior.division	19.6781	Left.Heschls.Gyrus..includes.H1.and.H2.	18.878
Left.Supramarginal.Gyrus..posterior.division	15.7818	Left.Inferior.Temporal.Gyrus..posterior.division	14.641
Right.Central.Opercular.Cortex	17.2968	Left.Inferior.Temporal.Gyrus..temporooccipital.part	24.317
Right.Heschls.Gyrus..includes.H1.and.H2.	13.1379	Left.Insular.Cortex	15.927
Right.Middle.Temporal.Gyrus..anterior.division	15.6176	Left.Intracalcarine.Cortex	35.249
Right.Middle.Temporal.Gyrus..posterior.division	15.253	Left.Lateral.Occipital.Cortex..inferior.division	22.746
Right.Parietal.Operculum.Cortex	12.510	Left.Lateral.Occipital.Cortex..superior.division	19.834
Right.Planum.Polare	14.949	Left.Lingual.Gyrus	32.404
Right.Planum.Temporale	12.617	Left.Middle.Temporal.Gyrus..temporooccipital.part	17.782
Right.Superior.Temporal.Gyrus..anterior.division	19.6635	Left.Occipital.Fusiform.Gyrus	24.141
Right.Superior.Temporal.Gyrus..posterior.division	18.8534	Left.Occipital.Pole	23.17
		Paracingulate.Gyrus	14.818
		Left.Parahippocampal.Gyrus..anterior.division	23.933

Left.Parahippocampal.Gyrus..posterior.division	30.177
Left.Parietal.Operculum.Cortex	19.769
Left.Planum.Temporale	20.791
Left.Precuneous.Cortex	25.556
Left.Subcallosal.Cortex	22.89
Left.Superior.Parietal.Lobule	13.534
Left.Supracalcarine.Cortex	34.165
Left.Supramarginal.Gyrus..posterior.division	19.854
Left.Temporal.Fusiform.Cortex..anterior.division	17.146
Left.Temporal.Fusiform.Cortex..posterior.division	25.091
Left.Temporal.Occipital.Fusiform.Cortex	30.718
Left.Temporal.Pole	15.41
Right.Angular.Gyrus	26.346
Right.Central.Opercular.Cortex	13.78
Right.Cingulate.Gyrus..posterior.division	23.764
Right.Cuneal.Cortex	26.278
Right.Frontal.Medial.Cortex	16.911
Right.Frontal.Orbital.Cortex	13.877
Right.Heschls.Gyrus..includes.H1.and.H2.	16.353
Right.Inferior.Temporal.Gyrus..anterior.division	15.577
Right.Inferior.Temporal.Gyrus..posterior.division	18.262
Right.Inferior.Temporal.Gyrus..temporooccipital.part	29.167
Right.Insular.Cortex	16.383
Right.Intracalcarine.Cortex	30.856
Right.Lateral.Occipital.Cortex..inferior.division	35.716
Right.Lateral.Occipital.Cortex..superior.division	19.643
Right.Lingual.Gyrus	27.537
Right.Middle.Temporal.Gyrus..posterior.division	16.15

Right.Middle.Temporal.Gyrus..temporooccipital.part	32.438
Right.Occipital.Fusiform.Gyrus	24.567
Right.Occipital.Pole	30.231
Right.Parahippocampal.Gyrus..anterior.division	20.351
Right.Parahippocampal.Gyrus..posterior.division	25.145
Right.Parietal.Operculum.Cortex	21.039
Right.Planum.Polare	14.552
Right.Planum.Temporale	21.152
Right.Postcentral.Gyrus	13.107
Right.Precuneous.Cortex	22.867
Right.Subcallosal.Cortex	18.68
Right.Superior.Parietal.Lobule	13.68
Right.Superior.Temporal.Gyrus..posterior.division	14.929
Right.Supracalcarine.Cortex	30.665
Right.Supramarginal.Gyrus..anterior.division	15.081
Right.Supramarginal.Gyrus..posterior.division	22.485
Right.Temporal.Fusiform.Cortex..anterior.division	17.436
Right.Temporal.Fusiform.Cortex..posterior.division	21.616
Right.Temporal.Occipital.Fusiform.Cortex	28.231
Right.Temporal.Pole	14.486

Supplementary Table 7. Spearman correlation of SD_{BOLD} with SD_{EEG} for each frequency band in young subjects (N=135). None of the pairwise correlations between SD_{BOLD} and SD_{EEG} were statistically significant.

ROI	rho SD_{DELTA}	rho SD_{THETA}	rho SD_{ALPHA}	rho SD_{BETA}
Left Angular Gyrus	0.005	0.015	0.014	0.071
Left Central Opercular Cortex	0.037	0.001	0.076	0.034
Left Cingulate Gyrus, anterior division	-0.090	-0.077	0.091	-0.028
Left Cingulate Gyrus, posterior division	-0.096	-0.048	-0.018	0.042
Left Cuneal Cortex	-0.166	-0.153	-0.040	-0.055
Left Frontal Medial Cortex	-0.009	-0.083	-0.105	-0.100
Left Frontal Operculum Cortex	-0.067	-0.128	0.074	-0.094
Left Frontal Orbital Cortex	0.035	-0.010	0.137	0.107
Left Frontal Pole	0.110	-0.018	-0.029	-0.052
Left Heschl's Gyrus (includes H1 and H2)	-0.019	0.029	0.112	-0.096
Left Inferior Frontal Gyrus, pars opercularis	0.040	-0.082	0.063	-0.091
Left Inferior Frontal Gyrus, pars triangularis	0.031	-0.114	0.064	-0.041
Left Inferior Temporal Gyrus, anterior division	0.035	0.023	0.099	0.012
Left Inferior Temporal Gyrus, posterior division	0.047	0.078	0.116	0.034
Left Inferior Temporal Gyrus, temporooccipital part	0.030	-0.002	0.025	-0.089
Left Insular Cortex	0.023	-0.134	-0.017	-0.077
Left Intracalcarine Cortex	0.018	0.028	0.072	0.032
Left Juxtapositional Lobule Cortex (formerly Supplementary Motor Cortex)	-0.050	-0.099	0.077	0.022
Left Lateral Occipital Cortex, inferior division	-0.048	-0.030	-0.078	-0.077
Left Lateral Occipital Cortex, superior division	-0.062	-0.081	0.018	-0.088
Left Lingual Gyrus	0.131	0.060	-0.022	-0.035
Left Middle Frontal Gyrus	0.041	-0.066	0.131	0.015
Left Middle Temporal Gyrus, anterior division	0.004	-0.063	-0.014	-0.173
Left Middle Temporal Gyrus, posterior division	0.115	0.005	-0.041	-0.029
Left Middle Temporal Gyrus, temporooccipital part	0.072	0.037	0.071	-0.092
Left Occipital Fusiform Gyrus	0.146	0.149	0.115	0.026
Left Occipital Pole	-0.017	0.052	0.036	0.035
Left Paracingulate Gyrus	-0.044	-0.087	-0.012	-0.036
Left Parahippocampal Gyrus, anterior division	0.024	0.021	0.121	0.027
Left Parahippocampal Gyrus, posterior division	-0.086	0.030	0.117	0.162
Left Parietal Operculum Cortex	-0.130	-0.064	0.039	-0.110
Left Planum Polare	0.030	0.018	0.073	-0.004
Left Planum Temporale	-0.066	0.009	0.120	-0.071
Left Postcentral Gyrus	-0.019	-0.032	0.139	-0.060
Left Precentral Gyrus	-0.015	-0.074	0.091	-0.056
Left Precuneous Cortex	-0.029	-0.070	0.107	-0.044
Left Subcallosal Cortex	-0.038	-0.087	0.034	-0.074
Left Superior Frontal Gyrus	-0.108	-0.139	0.027	-0.038

Left Superior Parietal Lobule	0.087	0.041	0.135	-0.084
Left Superior Temporal Gyrus, anterior division	-0.010	-0.074	0.033	0.064
Left Superior Temporal Gyrus, posterior division	-0.059	-0.045	-0.047	-0.087
Left Supracalcarine Cortex	-0.076	-0.071	0.036	0.016
Left Supramarginal Gyrus, anterior division	0.026	-0.060	0.001	-0.057
Left Supramarginal Gyrus, posterior division	-0.005	0.066	0.106	0.043
Left Temporal Fusiform Cortex, anterior division	0.188	0.120	0.051	0.031
Left Temporal Fusiform Cortex, posterior division	0.056	0.052	0.144	0.075
Left Temporal Occipital Fusiform Cortex	0.096	0.094	0.128	0.092
Left Temporal Pole	0.224	0.105	0.152	-0.010
Right Angular Gyrus	-0.010	0.025	0.010	0.046
Right Central Opercular Cortex	0.084	-0.015	0.068	-0.030
Right Cingulate Gyrus, anterior division	-0.079	-0.085	0.062	-0.046
Right Cingulate Gyrus, posterior division	-0.090	-0.048	-0.004	0.021
Right Cuneal Cortex	-0.118	-0.096	0.017	-0.074
Right Frontal Medial Cortex	0.042	-0.043	0.063	-0.050
Right Frontal Operculum Cortex	0.004	-0.017	0.089	-0.075
Right Frontal Orbital Cortex	0.085	-0.024	0.100	-0.032
Right Frontal Pole	0.149	-0.022	0.014	-0.061
Right Heschl's Gyrus (includes H1 and H2)	-0.085	-0.045	0.065	-0.071
Right Inferior Frontal Gyrus, pars opercularis	-0.020	-0.029	0.127	-0.138
Right Inferior Frontal Gyrus, pars triangularis	-0.047	-0.092	0.061	-0.170
Right Inferior Temporal Gyrus, anterior division	0.013	-0.018	0.058	0.028
Right Inferior Temporal Gyrus, posterior division	0.179	0.070	0.128	-0.048
Right Inferior Temporal Gyrus, temporooccipital part	0.106	0.068	0.177	0.093
Right Insular Cortex	-0.034	-0.087	0.043	-0.054
Right Intracalcarine Cortex	-0.063	-0.121	0.008	-0.065
Right Juxtapositional Lobule Cortex (formerly Supplementary Motor Cortex)	-0.040	-0.142	0.015	-0.049
Right Lateral Occipital Cortex, inferior division	-0.025	0.005	0.081	0.026
Right Lateral Occipital Cortex, superior division	-0.008	-0.037	0.044	-0.113
Right Lingual Gyrus	0.040	0.033	0.058	0.034
Right Middle Frontal Gyrus	-0.167	-0.083	0.063	-0.143
Right Middle Temporal Gyrus, anterior division	0.135	0.049	0.054	-0.113
Right Middle Temporal Gyrus, posterior division	0.002	0.080	0.191	0.060
Right Middle Temporal Gyrus, temporooccipital part	0.026	0.011	0.094	0.049
Right Occipital Fusiform Gyrus	0.095	0.039	0.022	0.007
Right Occipital Pole	0.019	-0.050	0.025	-0.036
Right Paracingulate Gyrus	-0.063	-0.041	0.034	-0.012
Right Parahippocampal Gyrus, anterior division	-0.027	-0.005	0.071	0.102
Right Parahippocampal Gyrus, posterior division	0.020	-0.037	0.037	0.024
Right Parietal Operculum Cortex	-0.066	-0.039	0.124	-0.075

Right Planum Polare	0.186	0.073	0.105	-0.021
Right Planum Temporale	-0.028	-0.043	0.074	0.070
Right Postcentral Gyrus	0.070	0.026	0.133	-0.056
Right Precentral Gyrus	-0.031	-0.047	0.134	-0.040
Right Precuneous Cortex	-0.099	-0.145	0.053	-0.200
Right Subcallosal Cortex	-0.084	-0.086	0.098	0.054
Right Superior Frontal Gyrus	-0.100	-0.158	-0.026	-0.116
Right Superior Parietal Lobule	-0.035	-0.067	0.080	-0.103
Right Superior Temporal Gyrus, anterior division	0.144	0.056	0.050	0.021
Right Superior Temporal Gyrus, posterior division	0.067	0.068	0.064	0.004
Right Supracalcarine Cortex	-0.004	0.049	0.089	0.065
Right Supramarginal Gyrus, anterior division	0.134	0.092	0.116	0.046
Right Supramarginal Gyrus, posterior division	0.058	0.055	0.096	0.052
Right Temporal Fusiform Cortex, anterior division	0.038	-0.019	0.013	0.142
Right Temporal Fusiform Cortex, posterior division	0.012	0.011	0.075	0.103
Right Temporal Occipital Fusiform Cortex	-0.013	0.018	0.115	0.098
Right Temporal Pole	0.135	0.006	0.044	-0.129

*$p_{FDR} < 0.05$; **$p_{FDR} < 0.01$; ***$p_{FDR} < 0.001$, 2-tailed*

Supplementary Table 8. Spearman correlation of SD_{BOLD} with SD_{EEG} for each frequency band in old subjects (N=54). None of the pairwise correlations between SD_{BOLD} and SD_{EEG} were statistically significant.

ROI	rho SD_{DELTA}	rho SD_{THETA}	rho SD_{ALPHA}	rho SD_{BETA}
Left Angular Gyrus	-0.118	-0.100	-0.001	-0.192
Left Central Opercular Cortex	0.129	0.132	-0.006	0.204
Left Cingulate Gyrus, anterior division	-0.043	0.175	-0.034	0.010
Left Cingulate Gyrus, posterior division	0.014	-0.077	0.012	-0.301
Left Cuneal Cortex	-0.134	-0.157	-0.096	-0.387
Left Frontal Medial Cortex	-0.165	-0.129	-0.265	0.061
Left Frontal Operculum Cortex	0.173	0.168	0.063	0.029
Left Frontal Orbital Cortex	0.085	0.192	0.020	0.021
Left Frontal Pole	0.038	-0.009	-0.044	-0.080
Left Heschl's Gyrus (includes H1 and H2)	-0.066	-0.152	-0.166	0.027
Left Inferior Frontal Gyrus, pars opercularis	0.039	0.041	-0.039	0.177
Left Inferior Frontal Gyrus, pars triangularis	0.107	0.113	0.033	0.086
Left Inferior Temporal Gyrus, anterior division	0.111	0.153	0.088	0.278
Left Inferior Temporal Gyrus, posterior division	0.072	0.040	-0.035	0.040
Left Inferior Temporal Gyrus, temporooccipital part	0.016	0.074	0.034	-0.066
Left Insular Cortex	0.225	0.042	-0.079	0.026
Left Intracalcarine Cortex	0.102	0.130	0.254	0.172
Left Juxtapositional Lobule Cortex (formerly Supplementary Motor Cortex)	-0.054	-0.175	-0.035	-0.059
Left Lateral Occipital Cortex, inferior division	0.036	-0.027	-0.057	-0.184
Left Lateral Occipital Cortex, superior division	0.130	0.033	0.013	-0.083
Left Lingual Gyrus	-0.181	-0.101	-0.044	-0.130
Left Middle Frontal Gyrus	0.159	0.161	-0.009	-0.008
Left Middle Temporal Gyrus, anterior division	-0.004	0.000	-0.012	0.349
Left Middle Temporal Gyrus, posterior division	-0.007	-0.073	-0.197	0.077
Left Middle Temporal Gyrus, temporooccipital part	0.042	0.203	0.128	0.015
Left Occipital Fusiform Gyrus	0.105	0.118	0.088	0.086
Left Occipital Pole	-0.212	-0.082	0.070	-0.203
Left Paracingulate Gyrus	-0.109	-0.024	-0.042	0.065
Left Parahippocampal Gyrus, anterior division	0.048	0.086	-0.069	-0.146
Left Parahippocampal Gyrus, posterior division	-0.012	0.058	0.062	-0.116
Left Parietal Operculum Cortex	0.151	-0.030	-0.036	-0.101
Left Planum Polare	0.041	0.075	-0.010	0.219
Left Planum Temporale	0.139	0.000	-0.060	0.079
Left Postcentral Gyrus	-0.015	-0.118	-0.082	-0.060
Left Precentral Gyrus	-0.131	-0.007	-0.045	-0.060
Left Precuneous Cortex	0.059	0.007	-0.004	-0.101
Left Subcallosal Cortex	-0.065	-0.078	-0.140	-0.002

Left Superior Frontal Gyrus	-0.020	-0.126	-0.050	0.026
Left Superior Parietal Lobule	-0.075	-0.023	0.028	-0.054
Left Superior Temporal Gyrus, anterior division	0.052	0.140	-0.072	0.148
Left Superior Temporal Gyrus, posterior division	-0.150	0.047	0.002	-0.093
Left Supracalcarine Cortex	-0.004	-0.077	0.181	-0.093
Left Supramarginal Gyrus, anterior division	0.029	0.005	-0.033	0.114
Left Supramarginal Gyrus, posterior division	0.167	0.100	0.090	-0.027
Left Temporal Fusiform Cortex, anterior division	0.045	0.076	-0.059	0.062
Left Temporal Fusiform Cortex, posterior division	-0.052	0.124	0.069	0.182
Left Temporal Occipital Fusiform Cortex	0.089	-0.049	-0.054	-0.100
Left Temporal Pole	0.015	0.073	0.025	0.187
Right Angular Gyrus	-0.015	-0.032	0.063	-0.074
Right Central Opercular Cortex	-0.120	-0.020	-0.063	-0.070
Right Cingulate Gyrus, anterior division	0.027	0.176	0.038	0.036
Right Cingulate Gyrus, posterior division	0.092	-0.058	0.051	-0.256
Right Cuneal Cortex	-0.111	-0.174	0.015	-0.224
Right Frontal Medial Cortex	-0.119	-0.072	-0.060	-0.011
Right Frontal Operculum Cortex	-0.032	-0.015	-0.019	-0.056
Right Frontal Orbital Cortex	-0.018	-0.040	-0.104	0.076
Right Frontal Pole	-0.018	-0.050	-0.095	0.058
Right Heschl's Gyrus (includes H1 and H2)	-0.025	-0.084	-0.079	-0.138
Right Inferior Frontal Gyrus, pars opercularis	-0.102	-0.050	-0.156	-0.094
Right Inferior Frontal Gyrus, pars triangularis	-0.215	-0.062	-0.185	-0.128
Right Inferior Temporal Gyrus, anterior division	0.038	-0.076	-0.097	-0.180
Right Inferior Temporal Gyrus, posterior division	0.069	-0.002	-0.071	-0.128
Right Inferior Temporal Gyrus, temporooccipital part	-0.153	-0.115	-0.171	-0.217
Right Insular Cortex	-0.035	0.031	-0.006	-0.068
Right Intracalcarine Cortex	-0.078	-0.140	-0.117	-0.088
Right Juxtapositional Lobule Cortex (formerly Supplementary Motor Cortex)	-0.013	-0.167	-0.114	-0.135
Right Lateral Occipital Cortex, inferior division	-0.055	-0.088	0.125	0.008
Right Lateral Occipital Cortex, superior division	-0.035	-0.078	0.043	-0.119
Right Lingual Gyrus	-0.180	-0.115	-0.096	-0.149
Right Middle Frontal Gyrus	0.117	0.014	0.102	0.055
Right Middle Temporal Gyrus, anterior division	-0.130	-0.068	-0.120	-0.126
Right Middle Temporal Gyrus, posterior division	-0.030	-0.033	-0.008	0.045
Right Middle Temporal Gyrus, temporooccipital part	-0.008	-0.071	0.010	-0.109
Right Occipital Fusiform Gyrus	0.115	0.249	0.163	0.237
Right Occipital Pole	-0.053	-0.067	0.074	-0.006
Right Paracingulate Gyrus	-0.062	0.123	0.042	-0.085
Right Parahippocampal Gyrus, anterior division	-0.093	-0.061	-0.033	-0.109
Right Parahippocampal Gyrus, posterior division	-0.105	-0.118	-0.103	-0.137

Right Parietal Operculum Cortex	0.105	-0.050	-0.019	-0.072
Right Planum Polare	-0.033	0.050	-0.042	-0.148
Right Planum Temporale	-0.064	-0.135	-0.057	-0.209
Right Postcentral Gyrus	-0.071	0.014	0.047	0.051
Right Precentral Gyrus	0.031	0.027	-0.039	-0.175
Right Precuneous Cortex	0.077	0.071	0.010	-0.035
Right Subcallosal Cortex	0.018	0.044	-0.007	-0.106
Right Superior Frontal Gyrus	-0.159	-0.162	-0.149	-0.156
Right Superior Parietal Lobule	-0.007	0.035	-0.001	-0.063
Right Superior Temporal Gyrus, anterior division	-0.155	-0.045	-0.124	-0.175
Right Superior Temporal Gyrus, posterior division	-0.133	-0.052	-0.127	-0.081
Right Supracalcarine Cortex	-0.131	-0.153	0.138	-0.174
Right Supramarginal Gyrus, anterior division	-0.101	-0.061	-0.078	-0.068
Right Supramarginal Gyrus, posterior division	-0.149	-0.079	-0.022	-0.222
Right Temporal Fusiform Cortex, anterior division	-0.005	0.064	-0.020	-0.041
Right Temporal Fusiform Cortex, posterior division	-0.095	-0.036	0.030	-0.137
Right Temporal Occipital Fusiform Cortex	-0.124	-0.080	0.002	-0.073
Right Temporal Pole	-0.181	-0.112	-0.230	-0.284

*$p_{FDR} < 0.05$; **p_{FDR}

Supplementary Table 9. Contributions of selected region of interests (ROIs) to each principle components (PCs) resulted from of the Singular Value Decomposition (SVD) analyses for SD_{BOLD}, SD_{DELTA}, and SD_{THETA}. ROIs derived from the previous fMRI literature, and their corresponding ROIs in Harvard-Oxford atlas to investigate the age-dependent relationship between TMT and SD_{BOLD} or SD_{EEG} (See: Table 1). As a criterion, the minimum total variance explained over 70% was selected (Jollife and Cadima, 2016), resulting in three PCs in SD_{BOLD} (52.82%, 10.34%, and 7%), two PCs in SD_{DELTA} (67.37%, 10.95%), and one PC in SD_{THETA} (75.63%).

	SD_{BOLD}			SD_{DELTA}		SD_{THETA}
Regions of Interest	PC1	PC2	PC3	PC1	PC2	PC1
Left.Cingulate.Gyrus..anterior.division	6.089654	10.83573301	0.57335642	6.293254	4.771	6.074438
Left.Cingulate.Gyrus..posterior.division	5.157258	10.43198257	14.34970502	5.512103	8.818	5.977285
Left.Frontal.Medial.Cortex	2.291563	7.93654130	10.93536588	3.528656	0.025	4.072425
Left.Insular.Cortex	6.077573	2.00659998	14.77254088	6.299486	2.866	6.054641
Left.Middle.Frontal.Gyrus	7.236614	1.52487430	0.87793136	6.234210	0.0249	6.137876
Left.Middle.Temporal.Gyrus..anterior.division	3.086762	17.51744070	6.19688362	5.172188	15.0212	5.003268
Left.Middle.Temporal.Gyrus..posterior.division	4.406356	15.17712851	3.05589786	5.799520	10.474	5.435104
Left.Middle.Temporal.Gyrus..temporooccipital.part	5.472472	0.04546836	2.61039871	4.196545	1.262	4.698550
Left.Precentral.Gyrus	6.217582	2.57399365	4.67714091	6.894773	0.0000	6.686272
Left.Superior.Frontal.Gyrus	7.381836	0.32612274	0.61245518	5.792227	5.0748	5.692948
Left.Superior.Temporal.Gyrus..anterior.division	4.947440	0.05546047	0.03483502	4.491588	18.9260	4.466424
Left.Superior.Temporal.Gyrus..posterior.division	5.338529	7.26165079	0.67087115	5.690691	12.248	5.451148
Right.Cingulate.Gyrus..anterior.division	6.152739	9.90571267	0.90070689	6.200047	5.448	6.070030
Right.Cingulate.Gyrus..posterior.division	5.192974	10.04779651	14.34718789	5.404548	9.346	5.913883
Right.Insular.Cortex	7.339789	0.25286095	0.58469394	6.523552	0.0871	6.381107
Right.Middle.Frontal.Gyrus	5.606567	0.89429285	1.19883860	5.608391	1.1479	5.755169
Right.Occipital.Fusiform.Gyrus	5.520859	1.04779909	16.02672218	3.929315	2.298	3.899637
Right.Precentral.Gyrus	6.483434	2.15854154	7.57446847	6.428907	2.1581	6.229797

Supplementary Table 10. Results of multiple linear regression analyses investigating the relationship between the principle components (PCs) in SD_{BOLD}, SD_{DELTA}, and SD_{THETA} derived from Singular Value Decomposition (SVD) and task completion time in Trail Making Test (Reitan, 1955; Reitan and Wolfson, 1995) as the dependent variable.

	SD_{BOLD}				**SD_{DELTA}**				**SD_{THETA}**			
	TMT-A		**TMT-B**		**TMT-A**		**TMT-B**		**TMT-A**		**TMT-B**	
	Beta	p-value	Beta	p-value	Beta	p-value	Beta	p-value	Beta	p-value	Beta	p-value
PC1	0.004	0.254	0.004	0.922	0.005	1	0.006	1	-0.007	0.804	-0.007	<0.001
Age	0.009	<0.001	0.015	<0.001	0.012	<0.001	0.009	<0.001	0.008	<0.001	0.01	<0.001
PC1 * Age	0.0002	0.592	0.0006	0.961	0.0001	0.481	-0.0002	0.325	0.0002	0.372	-0.0002	0.161
PC2	-0.017	0.961	-0.017	0.186	-0.011	1	0.003	0.764				
PC2 * Age	-0.0009	0.296	-0.002	**0.027**	-0.0005	0.362	-0.001	0.08				
PC3	0.02	0.142	0.019	0.282								
PC3 * Age	-0.0002	0.824	0.0003	0.556								